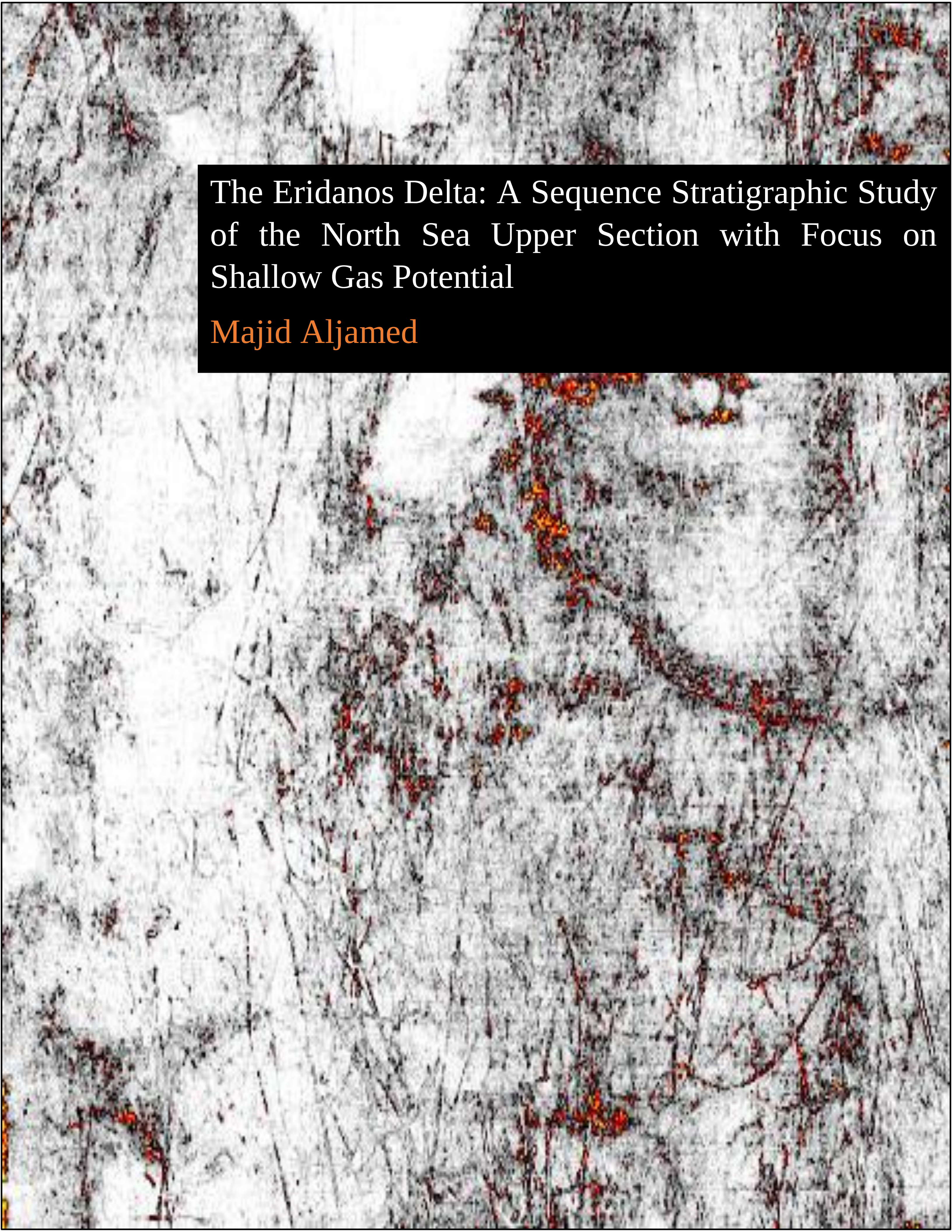

The Eridanos Delta: A Sequence Stratigraphic Study of the North Sea Upper Section with Focus on Shallow Gas Potential

Majid Aljamed

The Eridanos Delta: A Sequence Stratigraphic Study of the North Sea Upper Section with Focus on Shallow Gas Potential

Master Thesis

for obtaining the degree of Master in Applied Earth Science
by

Majid M. Aljamed
16th August 2018

Technical University of Delft, The Netherlands.
Faculty of Civil Engineering and Geoscience

Supervised by
Dr. Joep Storms

Committee
Dr. Hemmo Abels
Dr. Auke Barnhoorn

TU Delft Delft University of Technology

Acknowledgment

Having reached this point, I would like to express my sincere gratitude towards everyone who contributed to my success in obtaining my Master degree including the staff of TUDelft, family, friends and Saudi Aramco.

Special thanks to my supervisor Dr. Joep Storms, who took part in each phase of the project from step one, when it came to choosing a research topic that can both satisfy my learning curiosity and enhance my knowledge in a combined academic and operational manners. Joep made it possible to enjoy researching and replace feeling stressed and obligated with love to the subject and craving for better results. His unquestionable knowledge and experience surely enhanced my learning curve at TUDelft, making the thesis project the most knowledge bearing course of all. Above all, he always insisted that I have to work on topics of my interest and guided me through the research with such a unique character that is full of energy and positivity.

Would also like to thank the other committee members, Dr. Hemmo Ables for opening his doors for any questions and offering support when needed and immediately sharing any new articles that can benefit my research. Moreover, Dr. Auke Barnhoorn for not only taking part in my thesis committe but for teaching me great subjects in TUDelft especially in petrophysics that were really handy in my Master project.

Last but not least, I would like to express my gratitude to Saudi Aramco for sponsoring my studies and being there for me all the time providing support and making sure the experience in the Netherlands is well worth it. Having special place in my mind and heart, I would like to thank my ERAD family especially Ibrahim AlGhamdi and David Tang for their infinite effort in providing all the possible support to make me successful not only as an employee but even more as an individual.

Abstract

The Late Cenozoic Eridanos River brought vast amount of sediments to the North Sea Basin accumulating more than 1000m of deltaic deposits in less than 3.5 Ma. Since the gas discoveries in the shallow sediments were made, more attention is being paid to these deltaic deposits and that resulted in more data availability.

This study concentrates on the Eridanos Delta and identifies the properties of the delta in terms of its progadation distance and sedimentation rate and compare different time models to the ones provided by Overeem (2001) and Kuhlmann (2008). Furthermore, studies the reservoir rocks in terms of their petrophysical properties and facies distribution. Moreover investigates the reasoning behind the shallow sediments gas accumulations and factors behind the concentration of all the discoveries around the A and B blocks. Lastly, constructs a 3D model of the reservoirs distribution in the study area and their properties by integrating the study results of geological, geophysical, petrophysical and reservoir engineering data.

Such results were achieved by interpreting a high resolution 3D seismic survey and 2D lines in combination with wells' wireline logs and core data. Seismically, a total of 12 units were mapped to categories the successions (3.6 – 1.8Ma) that deposited post the Mid Miocene Unconformity. In addition, more than 20 wells were used to understand the reservoir properties in which seven wells have cores. Sedimentological aspects were assessed by studying the descriptions of cores and thin sections and the measurements of the core plugs. Gas accumulations were studied by evaluating the production data for gas and linking the gas to its source.

Contents

Figures

Tables

Appendix

Appendix A (Seismic structure maps)

Appendix B (Seismic isochrones maps)

Appendix C (3D modeling)

List of Abbreviations

MMU	Mid Miocene Unconformity
MGU	Mid Gelasian Unconformity
2D	Two Dimensions
3D	Three Dimensions
Ma	Million Years
Km	Kilometers
M	meters
ms	Millie Seconds
Ppm	Part Per Million
d	Day
N	North **S** South **E** East **W** West
SEG	Society of Exploration Geophysics
TD	Total Depth
TVD	True Vertical Depth
TDR	Time Depth Relation
UTM	Universal Transverse Mercator
RMS	Root Mean Square
TST	Transgressive System Tract
HST	Highstand Systems Tract
FSST	Falling Stage Systems Tract
LST	Lowstand Systems Tract
MFS	Maximum Flooding Surface
SB	Sequence Boundary

1.Introduction

Most studies of the stratigraphy of the North Sea Basin are focused on the hydrocarbon of the deep reservoirs (2-4 km). As the Upper North Sea Group was considered hazardous (Schroot, 2003), since it is gas bearing, very little interest was paid to it in terms of production potential. Post the Mid-Miocene Unconformity (MMU), vast amount of sediment was supplied to the North Sea Basin (Gibbard, 2014), in which further gas accumulations might have been trapped. Seven discoveries were already made, in which three fields from blocks A12, A18 and B13 are producing while the rest are still undeveloped. As the North Sea Basin hosts producing reservoirs from the Paleozoic and Mesozoic in addition to the relatively recent gas discoveries in the shallow sediments (Ten Veen, 2013), data availability with higher quality has become more accessible.

In the North Sea area, an uplift of up to 3km occurred, which is attributed to domal activities (Knox, 2010). With the ongoing subsidence in the North Sea Basin, drainage by rivers to the East and later to Southeast supplied huge amounts of coarse sediments (Gibbard, 2014) that contributed in forming gas bearing reservoirs. The shallow reservoir rocks are ascribed to the sediment supply by the Eridanos River of the Late-Cenozoic.

In this paper, comparison to previous work in addition to new results are provided. Previous studies were made on the area to understand the North Sea shallow sediments. Sedimentation rate was calculated by Overeem (2001) using a linear distribution based on one time control (10.7Ma). Another study by Kuhlmann (2006 and later 2008) calculated the sedimentation rate based on a linear distribution of three time controls (3.6Ma, 2.6Ma and 1.95Ma). This study experiments the effects of additional time controls, that were predicted by Kuhlmann (2008) and the original well A15-03 paleontological study by Verreussel & Jansen (1999), on sedimentation rate. Furthermore, based on the additional time controls, progradation distance was calculated to demonstrate the delta (formed by the Eridanos River) horizontal movement in time.

In addition to insights on previous studies, new results of the deltaic deposits were made. Investigation of the gas discoveries concentration around the A and B blocks was carried and common success factors of the discoveries were correlated. 3D model of the sand/silt bodies distribution and their properties was created. This was achieved by integrating results of different data sets. Geologically, sedimentological, and lithostratigraphic interpretations were made by analyzing cutting samples, descriptions of cores and thin sections (total of seven wells with cores in the shallow section were included). Geophysically, 12 seismic units were mapped on a high resolution 3D seismic survey in addition to 2D lines. Those units were used to establish a chronological order of the equivalent tops picked on well logs in time and then create a velocity model to link both. In addition, seismic attributes were generated to show depositional features that can explain the delta stages of development in time. Petrophysically, wireline log were interpreted in 20 wells to identify the properties of the mapped units in terms of sequence stratigraphic system tracts based on their gamma ray signature and use it to guide the litho-facies extrapolation. In addition, to populate the model with petrophysical properties (e.g. porosity and permeability), calibration between core plugs measurements and wells' wireline logs was made. Moreover, reservoir engineering data such as well tests and production data was used to examine the gas potential in the North Sea Basin shallow sediments and guide the core calibration with the appropriate fluid fill for the petrophysical calculations.

2. Geological Settings

While the main focus of the article is on the shallow (< 1 km) late Cenozoic successions that have the potential for gas accumulations, understanding the development of the North Sea Basin from early stages till the delta filling of the Cenozoic is important to recognize factors that affected the geometry of the basin early on and resulted in the origin and direction of the sediment supply.

2.1 Pre-Permian

Pre-Cambrian to Cambrian witnessed the formation of the Sub-Cambrian Peneplain. Some Cambrian crystalline rocks are present in the North Sea Basin at lower depths while Early Paleozoic is mainly characterized by volcanic clasts, basinal marine and metamorphosed rocks as a result of the Caladonian Orogeny (Cameron, 1993). Devonian deposits were mainly alluvial and the thickest section is in the east of Mid North Sea high (Ziegler, 1990). Three structure highs (Ringkobing, Fyn and Mid North Sea) became well established in the early Carboniferous times, as a result of crustal extension which lid to the deposition of up to 4000m of deep water and deltaic sediments in the subsiding grabens/ half grabens (Leeder, 1987). More sediments were deposited even during slow crustal extensions of the Mid to Late Carboniferous including the Lower Wesphalian coal, which is a main source rock of some gas fields in Sothern North Sea (Guion, 1988). At later stages of the Paleozoic, a chain of mountains, during the Variscan Orogeny, formed around the South North Sea making it a foreland area (Glennie, 1990). Overall, the two main events that attributed the most to the structure of the area during the Paleozoic are the Caledonian Orogeny (490-390Ma) and the Variscan Orogeny (370-290Ma). The resulted mountains and uplifted highs are the main sources of eroded sediments that filled the basin at later stages.

2.2 Permian to Triassic

In the Permian, the South North Sea was mainly surrounded by the Variscan mountains. The lower sediments of the Permian are less than 400m thick and compose mostly of aeolian and fluvial deposits (Cameron, 1993). For short times, some widespread transgressions of the Boreal Ocean affected the Late Permian. Those transgressions led to the development of some carbonates, marine shales followed by evaporates (Glennie, 1990). Most of those were severely deformed during basinal rifting and inversion of the Triassic, which also initiated salt diapers. Lower Triassic deposits were mainly muds and sands, which formed gas bearing reservoirs. The Mid and Late Triassic composed mainly of dolomites, anhydrites and widely spread halite (Fisher, 1990).

2.3 Jurassic to Cretaceous

North Sea first present day alignment of NNW-SSE was developed during the Early Jurassic crustal extension in which the Central Graben was formed and filled with more than 2000m thick sediments including organic rich shales (Figure 1). During the Mid-Jurassic lots of these sediments were eroded by domal uplifts that also slowed the subsidence of the Central Graben (Glennie, 1990). This uplift stopped and subsidence was renewed from the Late Jurassic to Early Cretaceous (Herngreen, 1987). The Jurassic sediments are mainly shallow marine and continental facies, which are overlain by argillaceous sediments in the Central Graben with thin organic rich shales (Brown, 1990). The lower Cretacous rocks are mainly marine carbonates and mudstones. By the Mid-Cretaceous, crustal extension ended but thermal anomaly it generated caused the North Sea Basin to continue subsiding (Cameron, 1993). At the end of the cretaceous, the fault bounded basin was subject to uplift and partial erosion. Those events of uplift and erosion triggered the deposition of up to 1500m of white-coccolith rich chalk separated by an unconformity from the overlaying Paleogene sediments, which records a general emergence of the area above sea level (Cameron, 1993). Following the renewed subsidence of the Palaeogene, nearly 1000m of argillaceous and marine sediment was deposited mainly above the Central Graben all the way soutward to the Netherlands, where only condensed sections accumulated in London Brabant Massif, Ringkobing and Fyn structure highs (Glennie, 1990).

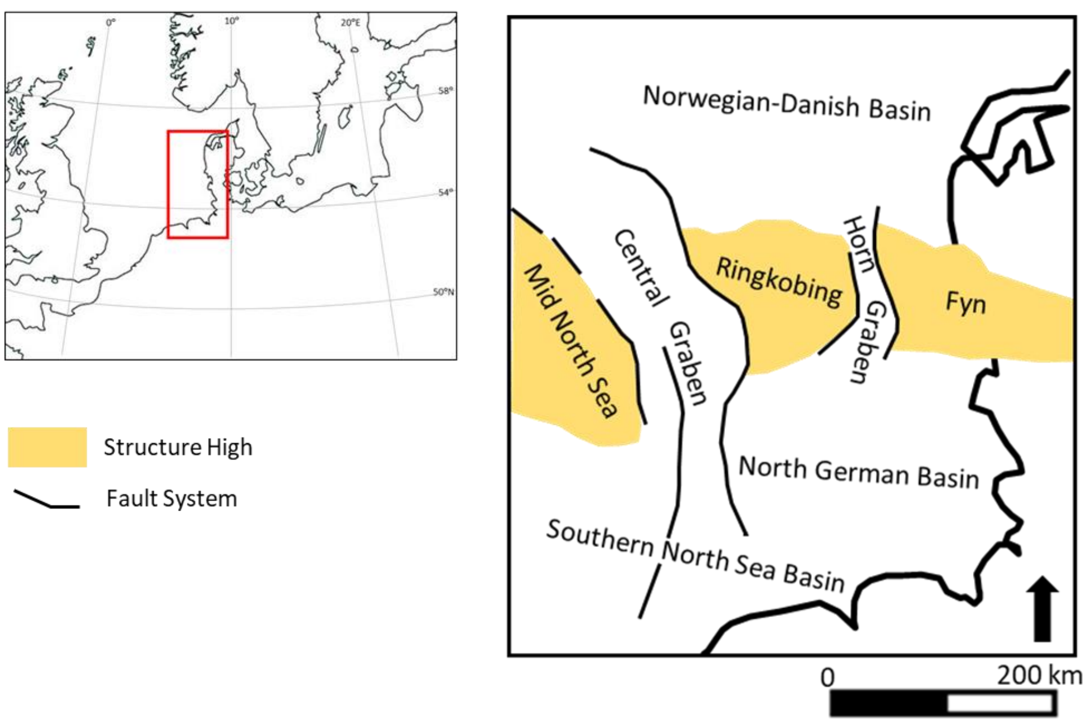

Figure 1: Mesozoic structure of the North Sea Basin (modified from Sorensen, 1997)

2.4 Paleocene to Oligocene

Early Paleocene had combined activities of both NW compressional stresses and regional uplift attributed to the rise of the Iceland mantle plume (Hillis, 2008). A significant uplift in Scandinavia also occurred and that activated drainage basin that discharged sediment and water towards S and SW (Gibbard, 2014). On the other side, more uplifts of the Scottish Highlands and the East Shetland Platform resulted in drainage to the East and filled the North of the North Sea Basin with more than 1000m of sediments. By the Late Paleocene, the sea covered big parts of East England, while most of the south North Sea Basin remained a low relief area (Gibbard, 2014).

During the Eocene, both a renewed thermal subsidence of the Northwest European Basin and the opening of the North Atlantic Ocean basin occurred (Gibbard, 2014). With the Viking Graben and Central North Sea being the main depocenters, lots of sediments deposited during the Eocene like London Clay which was sourced by the rivers from the North and West and later eroded and replaced by the expansion of fluvial deltas from the east during the Mid-Eocene (Knox, 2010). The Late Miocene was marked by regression from marginal areas of the basin caused by a regional uplift and local inversion of the basin (Gibbard, 2014).

The sedimentation during the Oligocene was more stable and most of it was caused by an uplift of the W and NE of the basinal margins. A new sediment source was resulted from a combined southward tilting and uplift of the Fennoscandian Platform, which created a N-S paleoslope that exposed land areas and marked a change from eastward to a westward progradation in North Sea (Gibbard, 2014). The Hiatus at Eocene-Oligocene is associated with the Pyrenean tectonic phase where a regional uplift and inversion toke place. More paleogeographic changes were subjected to the cooling events and the substantial glacio-eustatic fall in sea level during the Oligocene that was accompanied by renewal of tectonic activities (Miller, 1998). During this regression phase, large areas were subaerially exposed which allowed the extension of many rivers that supplied sediments from different directions into the basin (Gibbard, 2014) (Figure 2A).

2.5 Miocene to Pleistocene (The Development of Eridanos Delta)

Only during the Neogene, the Eridanos River was completely established (Figure 2B), which enhanced the sediment supply from the East and North. The catchment of the Baltic Rivers included the Baltic States and Fennoscandia (Knox, 2010). The Neogene was predominantly dominated by meandering rivers interpreted from the widespread fluvial sands and gravel which are associated with organic rich clay beds (Gibbard, 2014). During the Late Miocene, dramatic changes occurred in the North Sea Basin with rapid uplift of Fennoscandia. The uplift in Fennoscandia triggered erosion that led to major increase in sedimentation to SE on the North Sea Basin supplied by the Eridanos River. During the Miocene-Pliocene, channels dominated the pre-existing floodplains, with fluvial progradation arriving in the Netherlands at the end of Pliocene (Japsen, 2007). It is suggessted that during the Neogene, Norway was uplifted by as much as 2000m as an updoming continuation from the Paleogene and that was associated with the opening of the NE Atlantic Ocean. This allowed valley incisions to be dominant and cut up to 300m deep ,which increased dramatically later in the Quaternary (Lidmar-Bergstrom, 2000). The Eridanos River deposits, which were characterized by gravels, extended to the West during the Late-Miocene (Gibbard, 2014). A rise in relative sea level continued into Early-Pliocene as the North Sea Basin subsiding continued. Most of the sedimentation was caused by the Eridanos River, which led to a southward offshore progradation (Overeem, 2001). This effect of sea level rise was balanced in other parts by the continued uplift and erosion. The Pliocene is mostly characterized by braided rivers that supplied the catchments that dominantly formed during the Miocene by quartz dominated gravels and sands (Gibbard, 2014).

The delta formed by the Eridanos River, continued to expand West and Northwest during the Early-Pleistocene and that was attributed to the uplift of West, Northwest and North Britain (Overeem, 2001). Alternation in climate derived the deposition of the region with major glaciation occurring form Pliocene-Pleistocene that encouraged erosion and increased river incision (Figure 2C). The Rhine depositional fill became particularly important during the Middle-Pleistocene where its deltaic deposits covered central and southern North Sea (Gibbard, 2014). A barrier was formed to the South and separated North Sea from the channel. The Eridanos river system was disconnected from the Fennoscandian head-waters to the East. The Baltic basin was formed on the same time, which is attributed to erosion of ice sheets. Sediment supply still reached to the North Sea area by the Rhine, Meuse, Thames and Scheldt rivers during Mid-Pleistocene (Gibbard, 2014).

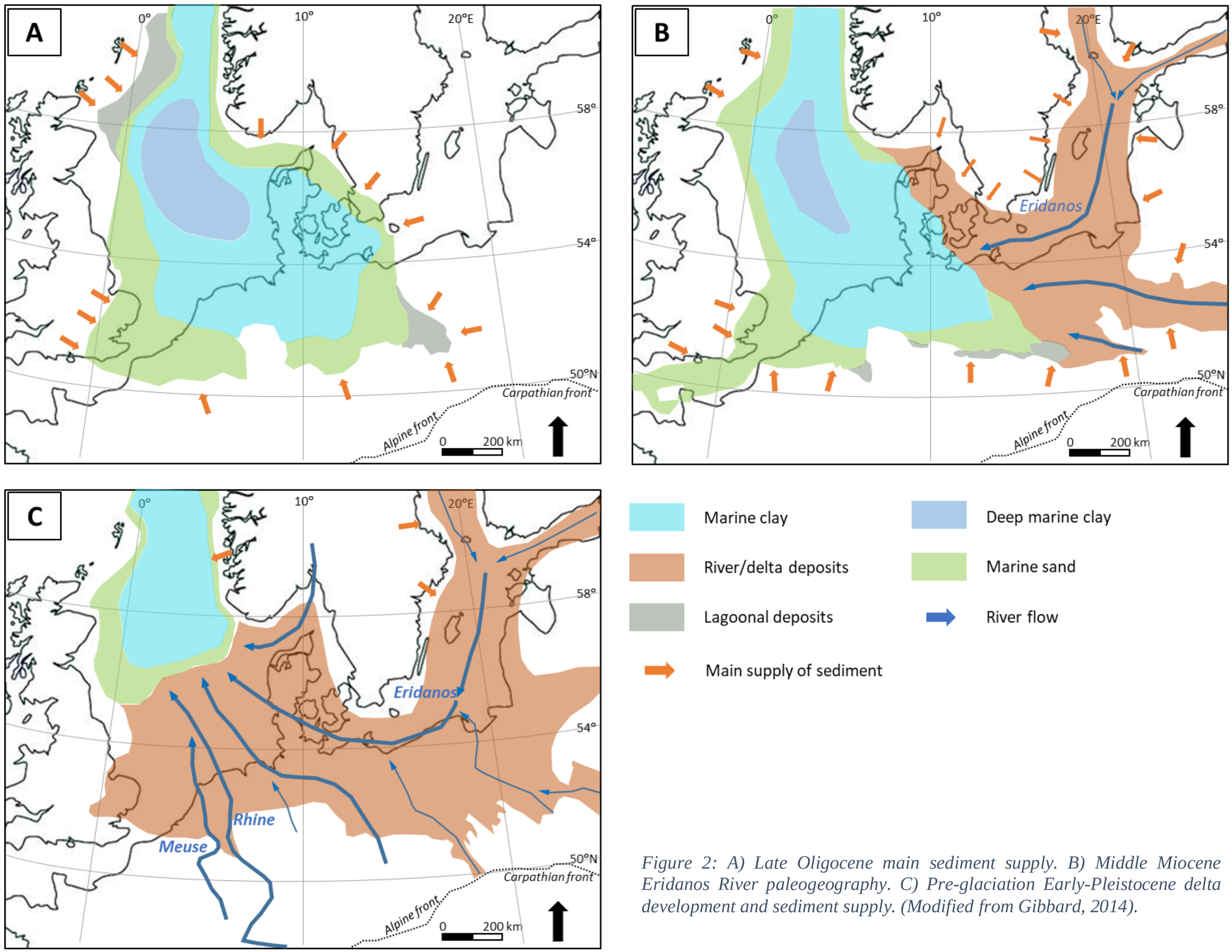

Figure 2: A) Late Oligocene main sediment supply. B) Middle Miocene Eridanos River paleogeography. C) Pre-glaciation Early-Pleistocene delta development and sediment supply. (Modified from Gibbard, 2014).

3. Area of Interest and Data Used

The area of interest was selected based on three criteria. Firstly, presence of gas at shallow depths (< 1 km) has to be confirmed. Secondly, high resolution seismic 3D survey has to be covering some of the discoveries. Lastly, the area needs to have a number of wells that penetrate the MMU with reliable wireline logs and preferably some core data (Figure 3).

Different data sets have been interpreted and integrated in the project some of which have high vertical resolution (e.g. wells and cores) and others that are primarily used to examine the lateral extent of the depositional facies (e.g. 2D and 3D Seismic) and those were mainly used for sedimentlogical, sequence stratigraphical and chronostratigraphical correlations. Other key sources of information such as hydrocarbon shows (e.g. high mudgas readings, which indicates higher carbon content) and flow tests performed in some wells were used to indicate specific potential zones and allow further examination of their properties and hence comparison with other prospective zones.

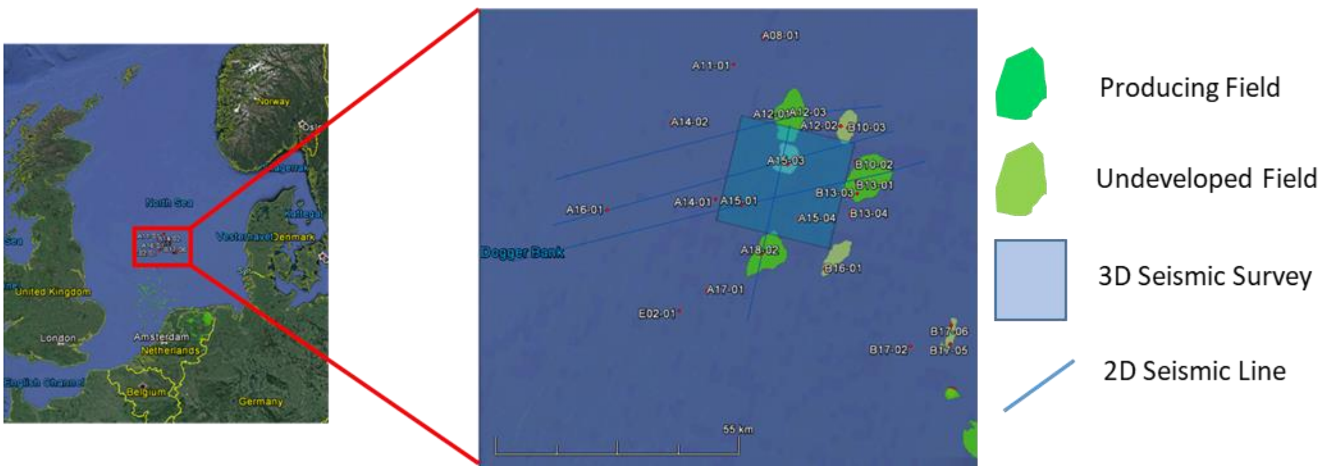

Figure 3: Area of interest and data used in the interpretation.

3.1 Well Data and Petrophysics

A total of 20 wells were used in the project for petrophysical correlation. Of those wells, 8 are intersecting seismic data thus been used to generate seismic seismograms and calibrate with available seismic data. Cored intervals in the shallow section are rare and in different intervals but present in seven of the wells, so core plugs data (porosity, permeability, density and formation factor) and lithological description were used. Of all the wells, 14 penetrate deeper than MMU, while the other 6 wells, have TD's (total depth) in shallower intervals (Table 1).

Well Name	**Intersecting Seismic**	**Core**	**Penetrating MMU**
A12-01	**2D**	X	✓
A12-02	X	X	✓
A12-03	X	✓	X
A14-01	X	X	✓
A14-02	X	X	✓
A15-01	**2D & 3D**	X	✓
A15-02	**2D & 3D**	X	X
A15-03	**3D**	✓	✓
A15-04	**3D**	✓	X
A16-01	**2D**	X	✓
A17-01	X	X	✓
A18-02	**2D**	✓	✓
B10-03	X	✓	✓
B13-01	**2D**	X	✓
B13-03	X	X	✓
B13-04	X	X	X
B16-01	X	X	X
B17-05	X	✓	✓
B17-06	X	✓	X
E02-01	X	X	✓

Table 1: Used well data in the area of interest.

3. 1.1 Core data

Core plugs measurements and core descriptions are available for the seven cored wells in the North Sea shallow section (< 1 km). An extensive study of well A15-03, including core description and thin section analysis was done by Van Den Belt (2000). Cores show alternation of very fine and coarser grains (Figure 4) and thin sections confirm lithofacies from both shallow marine and deeper marine environments (Figure 5). Measurements of core plugs were done for porosity, permeability, density and formation factor and the measurements data was used in this study to create two plots. The first plot shows the variation of porosity with depth (Figure 6) and the second is a plot of the porosity versus permeability in the North Sea shallow section (Figure 7). Interpretation of these data and their contribution in understanding the reservoir properties is discussed in (Chapter 6.3 Reservoir Characteristics).

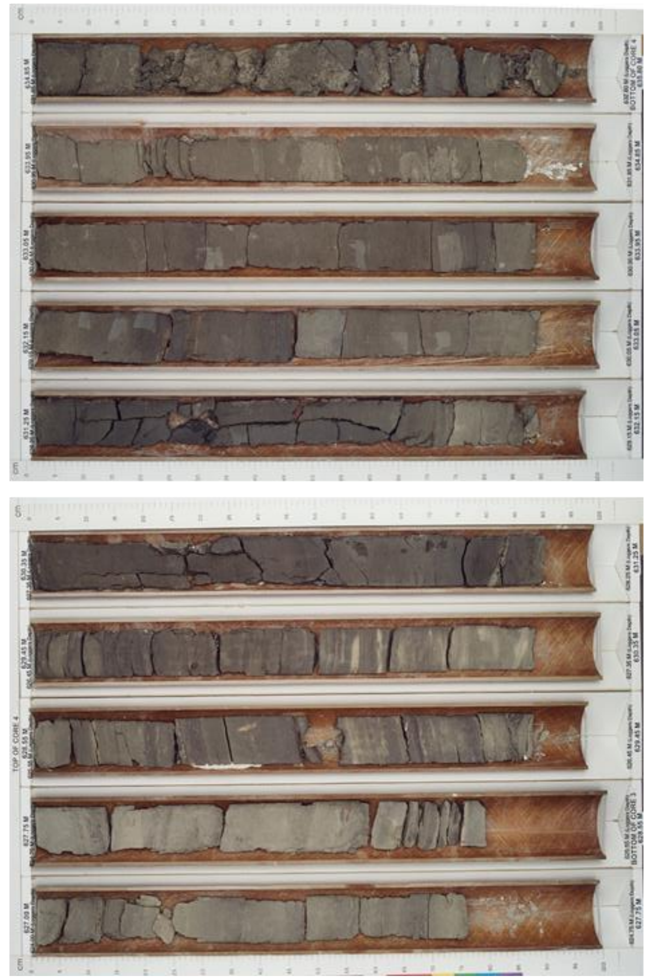

Figure 4: Thin sand reservoir intervals interbedded with silts and shales (Well A15-03 drilled by Wintershall, photos obtained from Nlog.nl)

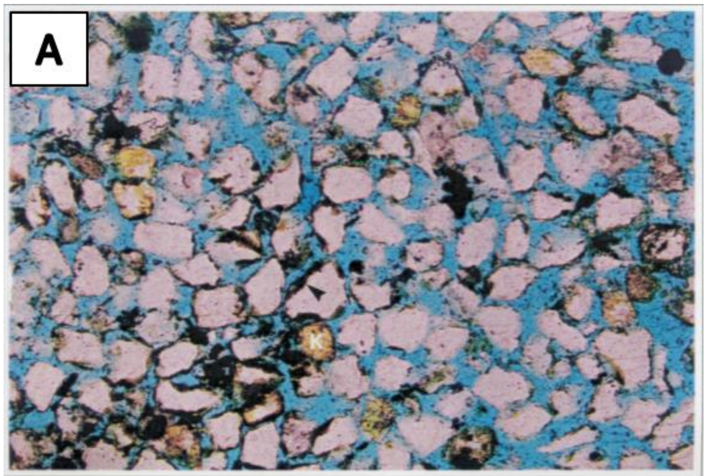

Magnification x 113 Depth: 485.00m 200µm

A) Very well sorted sandstone with a lack of detrital clays. K-feldspar (K) is common in the section. Grains are subangular to subrounded.

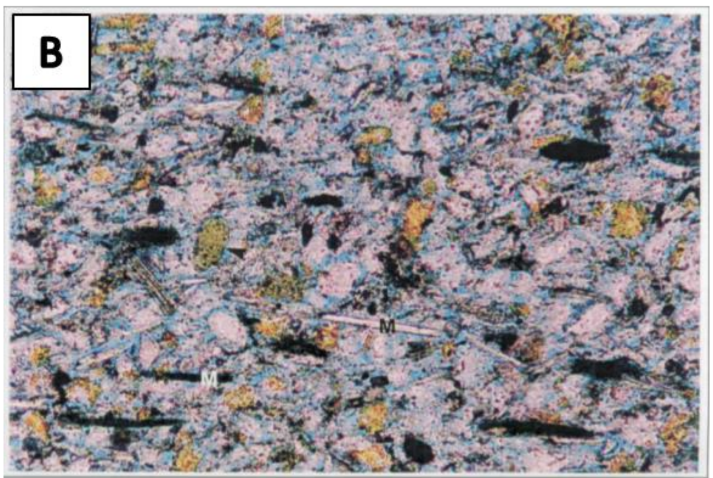

Magnification x 225 Depth: 616.28m 100µm

B) Well sorted clean siltstone with abundant mica (M), both muscovite and biotite, and K-feldspar. Rare abundance of glauconite is observed.

Magnification x 225 Depth: 826.00m 100µm

C) Pure claystone with rare silt grains and organic matter flakes. High micro-porosity is expected within the detrital clay matrix.

Figure 5: Thin sections of the observed lithofacies in well A15-03 varying from best reservoir sandstones at (A), silt and clays at (B) and deep marine clays at (C). View is using Plane Polarized Light. modified from the petrography report by Van Den Belt, 2000.

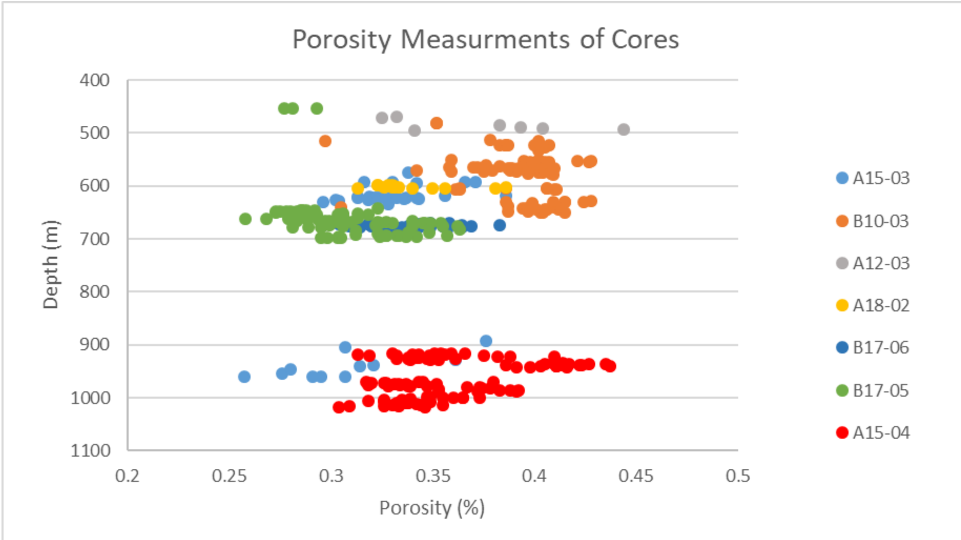

Figure 6: Porosity measurements of the seven wells that have cores in the shallow section of the North Sea Group plotted against depth in TVD (measurements from nlog.nl).

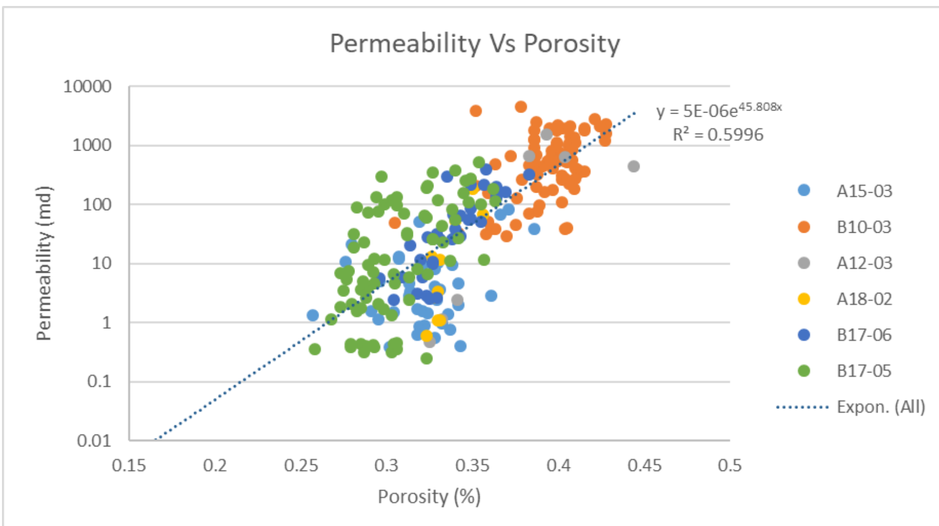

Figure 7: A directly proportional relation between permeability and porosity measurements from the cores of the shallow section of the North Sea Group (measurements from nlog.nl).

3.2 Seismic 2D and 3D

Both 3D and 2D Seismic data were used in the project. The main Seismic survey is Z3WIN2000A, which is in UTM31 (UTM: Universal Transverse Mercator). The seismic cube was released in 2010, is migrated and covers an area of around 615 km^2. A good vertical resolution of around 13ms which rounds up to approximately 9m is observed in the upper section. This is calculated by counting the number of cycles, which is peak to peak or trough to trough (Figure 8) in a certain window (200ms is used here) and then convert the cycle observed to meters using the interval velocity of the tops above MMU using equations 1 & 2 (Rafaelsen, 2006).

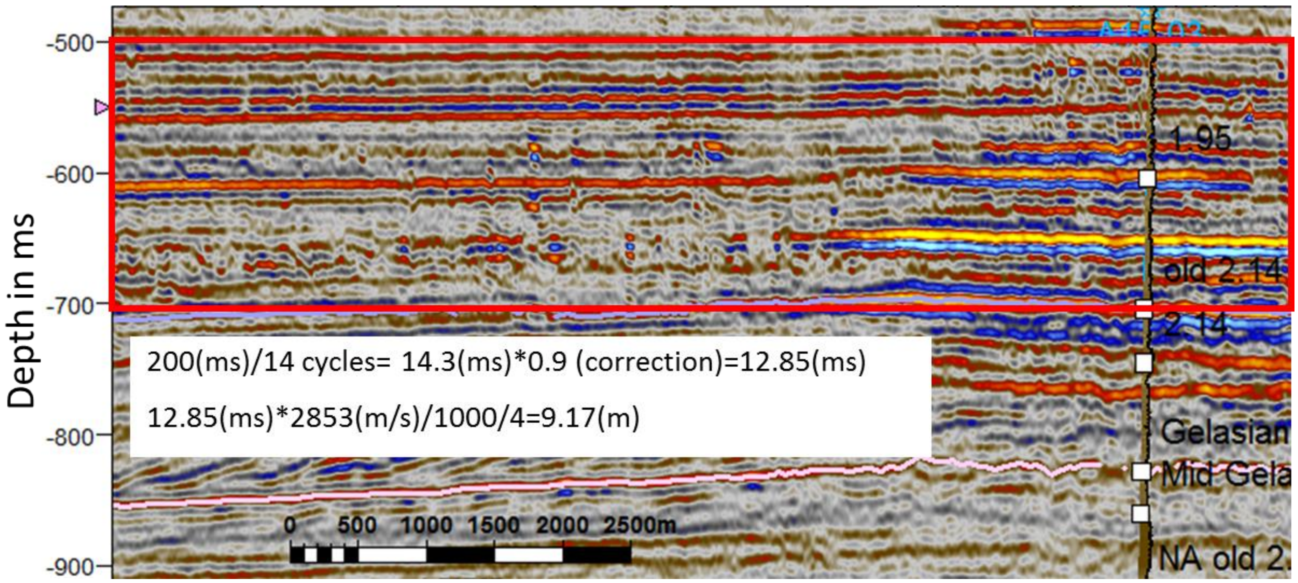

Figure 8: Defining frequency based on full cycles on a time window (200ms for this calculation); red is hardkick following the non SEG polarity conversion.

Equation 1: Calculating the wavelength (λ), based on the velocity (V) and the frequency (F)

$$\lambda = \frac{\mathrm{V}}{\mathrm{F}}$$

Equation 2: Calculating the resolution by using Rayleigh's criterion

$$Vertical\ resolution = \frac{\lambda}{4}$$

The 2D data interpreted in the project is composed of 4 main seismic lines (Table 2) that pass though the 3D seismic and extend the interpretation. Line AB-23 is more of a strike oriented to the Eridanos Delta (perpendicular to the sediment supply direction) while the other three are representative of a depositional dip direction in which the sequences stacking patterns are visible.

2D	Survey	Lat	Long	Type	Length (m)
SNSTI-NL-87-02	Z2NOP1987A	55°09'10.2604"N 55°27'43.9742"N	3°03'0.5072"E 4°06'0.8111"E	Migrated	74855.9
ABT-91-03	Z2NOP1991A	55°03'45.1546"N 55°25'11.3963"N	3°04'49.9120"E 4°09'32.0399"E	Migrated	78720.8
SNSTI-NL-87-03	Z2NOP1987A	54°58'15.8717"N 55°22'41.9078"N	2°58'26.9441"E 4°17'32.1334"E	Migrated	95051.4
AB-23	Z2WES1988B	54°58'44.9793"N 55°22'40.7095"N	3°47'36.7660"E 3°49'38.9804"E	Migrated	44442.4

Table 2: Details on the 2D seismic used in the project.

3.3 Hydrocarbon Indicators and Tests

Since the discovery of gas in the shallow North Sea section, some exploration wells have been drilled and resulted in the discovery of seven fields. Three of these are in blocks A12, A18 and B13 and are producing, while the discoveries in blocks A15, B10, B16 & B17 are still undeveloped. Production rates of the gas in the North Sea shallow section are proved to be as high as 1955 $10^6 m^3$/Month and that's obtained through horizontal wells to maximize the contact with the reservoir.

Hydrocarbon indicators of the shallow section are very limited as little attention was paid since the deeper sediments have very prolific hydrocarbon systems and the main focus was directed on them (Van Den Belt, 2000). For the purpose of identifying possible hydrocarbon potentials, three main indicators were investigated in 9 wells in terms of their reported core shows, production tests and mudgas readings (Table 3). The most reliable of the three is production test as cores could have some light stains or gas smell while mostly it's hard to detect. Mudgas is typically used to not just evaluate the abundance of hydrocarbon but even to characterize its type through the C1-C10 composition (Mode, 2014). In Addition, 15 horizontals' production rates and their reservoir zones were added up to know which reservoir zones are more prolific and in which areas the petroleum system isn't as functional (Table 4).

Well	Core Disc.	Test	Interval TVD (m)	Details
A12-03	X	✓	897 - 893	no flow
			553 - 575	max 307 $10^3 m^3$/d
A15-03	✓	✓	905 - 1000	less than 1000Nm^3/d
			598 - 669	up to 300
A15-04	✓	Mudgas	436 -442	6451 ppm
			632 - 740	max 7958 ppm
			920 - 1100	max 7629 ppm
			8914	9087 ppm
A18-02	✓	✓	600 - 610	318 $10^3 m^3$/d
			649 - 662	106 $10^3 m^3$/d d
B10-03	✓	✓	597 - 591	245 $10^3 m^3$/d
			514 - 510	420 $10^3 m^3$/d
B17-05	X	✓	676 - 664	100 $10^3 m^3$/d
			675	80000 ppm
B17-06	✓	Mudgas	560	2199 ppm
			772	12117 ppm
B13-03	X	✓	653 - 644	344 $10^3 m^3$/d
			544 - 530	185 $10^3 m^3$/d
B16-01	X	✓	660 - 658	267 $10^3 m^3$/d
			519 - 517	110 $10^3 m^3$/d

Table 3: Wells used for hydrocarbon shows identification (data from nlog.nl).

Well	Duration	Average Production rate in $10^6 m^3$/Month	Owner
A18			**Petrogas E&P Netherlands**
A18-A-01	02/16 - 02/18	14.3	
A18-A-02	12/15 - 02/18	17.2	
A18-A-03	01/16 - 02/18	15.8	
A18-A-04	07/17 - 02/18	6.0	
A12			**Chevron**
A12-A-01	12/07 - 02/18	284.4	
A12-A-02	01/08 - 02/18	1955.2	
A12-A-03	01/08 - 02/18	831.8	
A12-A-04	10/08 - 02/17	620.5	
A12-A-05	01/08 - 07/17	86.9	
A12-A-06	12/07 - 01/17	1129.8	
A12-A-07	12/07 - 02/18	629.6	
B13			**Chevron**
B13-A-01	12/11 - 02/18	15.1	
B13-A-02	12/11 - 12/16	13.1	
B13-A-03	01/12 - 02/18	13.7	
B13-A-04	01/12 - 11/17	10.8	

Table 4: Production wells used to estimate the gas production rate per month (data from nlog.nl).

4. Methodology and Data Interpretation

As a variety of data sets were used, many stages required going back and forth for the modification of interpreted data. The most common comeback is the cross correlation between picks done on seismic data and wells' petrophysical logs. One of the pitfalls that is easily mistaken is following wireline logs signatures and assuming the system has a layered cake correlation. Usually such interpretation in clastic systems, especially deltas, lead to false results and losing the chronostratigraphic scheme to a lithostratigraphic one. This section demonstrates the main seismic and well data methodologies and interpretation techniques, while some extra methodologies for stratigraphic interpretations and establishing a 3 model will be covered in their designated sections.

4.1 Seismic Interpretation

Along with paleontological data for age control, seismic reflections provide one of the best lateral continuities of chronostratigraphic events (Eberli, 2002). Essentially, as seismic is provided in time, some well control is crucial for establishing a time/depth relation (TDR) before starting the horizon interpretation. This doesn't just grant a good understanding of the stratigraphic events and what they mean on seismic but later can be used in well correlation as reference well tops, since those were verified by seismic to be chronologically reliable. Moreover, after picking the seismic events, the extraction of seismic attributes, which is any quantity that is measured from seismic data, can provide additional insights to structural and sedimentological features that are used in reservoir characterization (Subrahmanyam, 2008).

The seismic picking was done using Non-SEG display (SEG: Society of Exploration Geophysics), where the red color represents seafloor when impedance (product of velocity and density) changes as we go from water to rock (Nietzsche, 2005).

4. 1.1 Generating synthetics

The aim of generating synthetics seismograms is to superimpose the wells, which are in feet or meters, on seismic, which is in time. To do so, a TDR needs to be established. Few methodologies can be used to reach such relation. The one followed in this study is using a Butterfly Wavelet and using sonic velocity and density logs to convert time to depth using the velocity of the layers. Well checkshots, whenever available, were used to enhance the time depth curve (Cunningham, 2000). After establishing the TDR, matching the seismic trace with the generated synthetic seismogram was done by comparing the two logs and see how correlatable the two are. In rare cases when the sonic calibration wasn't established properly, some manual shift was performed to result into a reasonable correlation.

4. 1.2 Picking seismic horizons

The very first step for picking seismic horizons, is to create an arbitrary line that connects the wells with generated synthetics to check if all the provided stratigraphic intervals are matching. To do so, a careful match of the depth in seismic 2D lines and 3D needs to be done, usually using depth shift by matching a clear event that is correlatable across all lines. Two unconformities were used as base for picking the seismic events in this study. One is the Mid Miocene Unconformity (MMU), which is the main unconformity that is used to mark the start of the shallow North Sea sediments (Overeem, 2001). The MMU is recognized mostly on seismic by its discontinues reflection that varies in amplitude laterally with all the layers onlapping on it. Picking the MMU on well logs is possible, however, there is no absolute consistent characteristics as the unconformity eroded different layers at different depths, so guidance using seismic picks is needed. The second unconformity, which formed during the Mid Gelasian (MGU), is identified both seismically with regressive clinoforms downlapping on it and from wireline logs with a sudden shift from high to low gamma ray, which indicates coarsening upward (Glover, 2000). After this composite line was created and checked for depth consistency between the wells, the targeted horizons were picked starting with the seismic events that have the highest amplitude and more lateral continuity. The starting point for any horizon picking, when wells are available, should be from the well location and extended gradually to other wells, to guaranty consistency between well tops and seismic horizons. Once all the targeted seismic events were picked, the interpretation on the arbitrary line was used as a reference for all the seismic data including the 2D lines and 3D survey. As the 3D block falls in between the four 2D lines (Figure 3), the 2D lines were picked first and then extended in the 3D cube from the crossing points. When two subsequent horizons are laterally continues and can be linked to clear changes in well petrophysical logs, the bounded sediment in between is called in this study a seismic unit.

4. 1.3 Seismic attributes

Many features can be obtained by generating seismic attributes. Some are directly related to physical properties that are extracted from wave propagation and some are geometrical that are related to dip and continuity of the events on seismic (Subrahmanyam, 2008). In this study, three different kinds of seismic attributes were generated to further understand and map the geological features of the 3D survey. The first attribute is RMS amplitude (RMS: Root Mean Square), which is an averaging method taking the square root of all the waveform square values (Koson et al., 2014). RMS amplitude is often used for the detection of pressure zones and velocity variation that can infer change in density and lithology (e.g. sand and shale) (Subrahmanyam, 2008). The second attribute is the envelope (known as reflection strength), which highlights main seismic events by calculating a complex trace of the signals. This attribute displays bright events independent of the polarity, which is good to show discontinuities, variation in lithologies and bright spots (Koson et al., 2014). Variance is the third attribute, which is helpful in mapping channels and for the delineation of faults, and is calculated by measuring the waveforms similarity over a given time or window (Koson et al., 2014).

4.2 Well Correlation

The base for picking the well tops is taken from the correlation provided by Kuhlmann (2006), those picks are the ones initially used for the wells in synthetics generation. As seismic interpretation was done, the correlation between wells was modified based on the seismic chronostratigraphic interpretation, then extended to other wells. Wells that cross seismic lines (Table 1) were correlated first, to provide a control that match both the petrophysical signature and seismic trace. Whenever core data is available, the wells are given priority, as core provide the best high vertical resolution for sedimentological correlation. Six main wireline logs were used in correlating the wells. Those are gamma ray, caliper, sonic velocity, neutron porosity, density and resistivity. Gamma ray, which measures the natural radioactivity by determining the decay of atoms, is mainly used to identify shales (Glover, 2000). Caliper log, which measures the hole diameter to insure consistency in other measurements that can be affected by caving or enlargement of drilling hole (Serra, 1984). Sonic velocity, which measures the velocity of the formation, is used to determine the porosity and needs to be combined with other logs to differentiate between clay fill or fluid fill of the pores (Serra, 1984). Neutron porosity is used to determine the total porosity by measuring the hydrogen concentration in the formation (Glover, 2000). Density log measures the bulk density of the formation and is used for porosity, lithology identification and compaction (Glover, 2000). Resistivity is a measure of the conductivity in the formation and is the main wireline log that is used to determine the fluid fill of the pores (Serra, 1984).

5. Chronostratigraphy and Paleoenvironment

Chronostratighrapy is directly linked to the interpretation of seismic data, since the continuity of seismic reflections can indicate that those events are time equivalent (Eberli, 2002). A total of twelve units were mapped seismically, five units which are between the MMU and the MGU and seven units that deposited above the MGU (Figure 9). Time controls are extended from the studies by Verreussel & Jansen (1999) and Kuhlmann (2006) for the relative age of the seismic units, which is based on eight boreholes in combination with paleomagnetic records. Not all units have solid age control, but some have bio-indicators and those were primarily used in the chronostratigraphic correlation. Three groups of fossils were used in the study, which are Dinoflagellate cysts (Dinocyst), pollen and foraminifers (foram). The base of the units is the MMU which is believed to occur around **12Ma**. Unit two is a thick interval that is predicted to extend from Zanclean to Piacenzian. Age of the unit is determined by R. actinocoronata (dinocyst) paleomarker of the Zanclean, that is approximately **3.5Ma**. The Top is marked by the appearance of I. Multiplexum (dinocyst) and disappearance of Barssidinium (dinocyst), which are indicators of Piacenzian. Top of unit 4 is dated to **2.4Ma** and that's marked by N. Atlantica (foram). The Gelasian, which is a thick interval, extends all the way to the top of unit 8. The abundance of A. Umbracula (dinocyst) that diminishes on the top of unit is used as the dominant biomarker of the Gelasian. The base of Olduvai is dated to **1.94Ma** and the age is marked by the occurrence of A. Filiculoides (pollen). Some events such as the MGU were not dated by biomarkers or paleo-magnetic indicators, however, relative age was assigned by the stratigraphic occurrence on wells and seismic sections.

Paleoenvironment interpretation was carried out by tying the fossils to the appropriate environmental condition where these are most abundant. This is mainly extended from the work done by Kuhlmann in 2006. Fossils used are sensitive to changes in the environment, where their abundance and density show good correlation with some key parameters such as the sea surface temperature, the state of the ocean (open marine, restricted..etc), the salinity and vegetation (Gibson, 1980). Units 1&2 mark the filling of the basin, following the MMU where the basin is fairly deep under open marine conditions, with fine grains composed mostly of silts and shales. Units 3&4 are on the transition to a more restricted settings. Variation of salinity caused different fossils to coexist while the alternations of warm and cold conditions is the main reason behind the generation of strong bottom currents that resulted in a N-S incisions. Units 5&6 were deposited in restricted marine conditions with cooling down on the top of unit 6. Sea level fall resulted in the formation of regressive clinoforms that are oriented ESE-WNW. Units 7-10 mark the major prograding delta wedges with shallow marine under arctic conditions. Sever scouring marks are observed on the sea floor as a result of iceberg movements. Units 11&12 are more of filling phases followed by fluvial in nearshore under arctic conditions (Figure 10 & Figure 11). At shallower depths, more valleys are observed, some of which can be classified as tunnel valleys and others are purely fluvial, which is mainly interpreted from the shape of the valley (Livingstone, 2016).

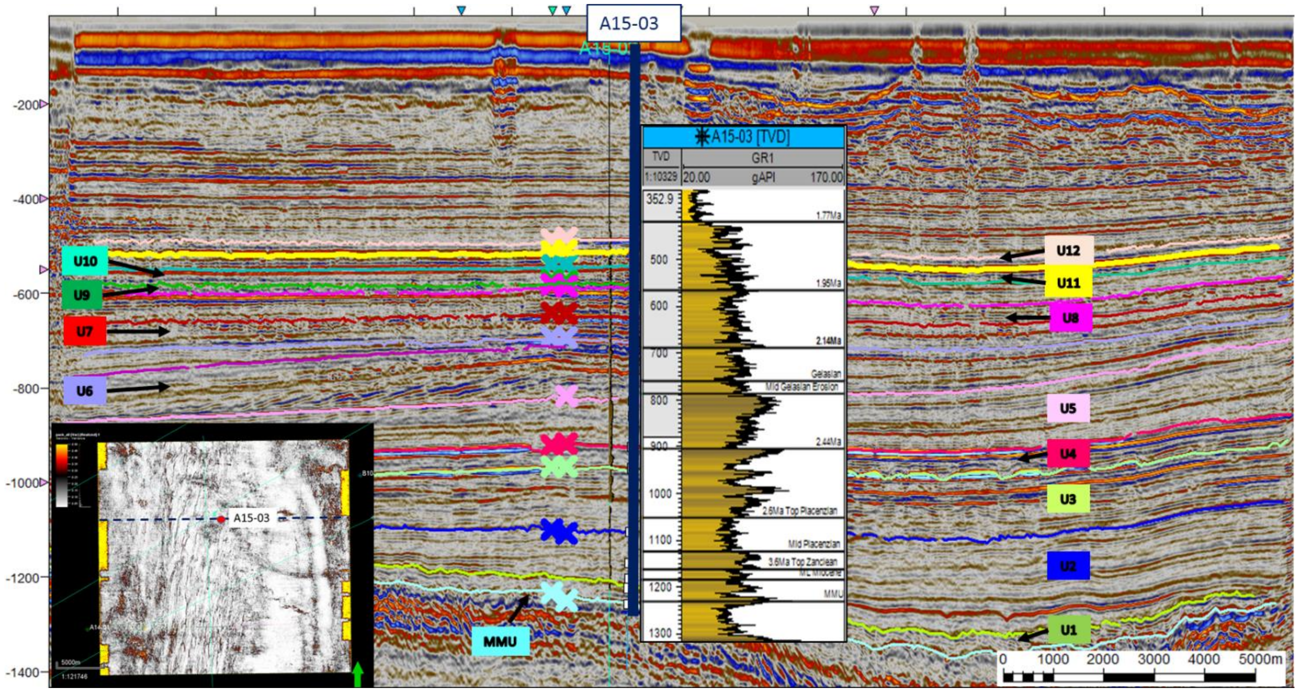

Figure 9: Seismic units picked in inline 3270 of the 3D survey passing well A15-03.

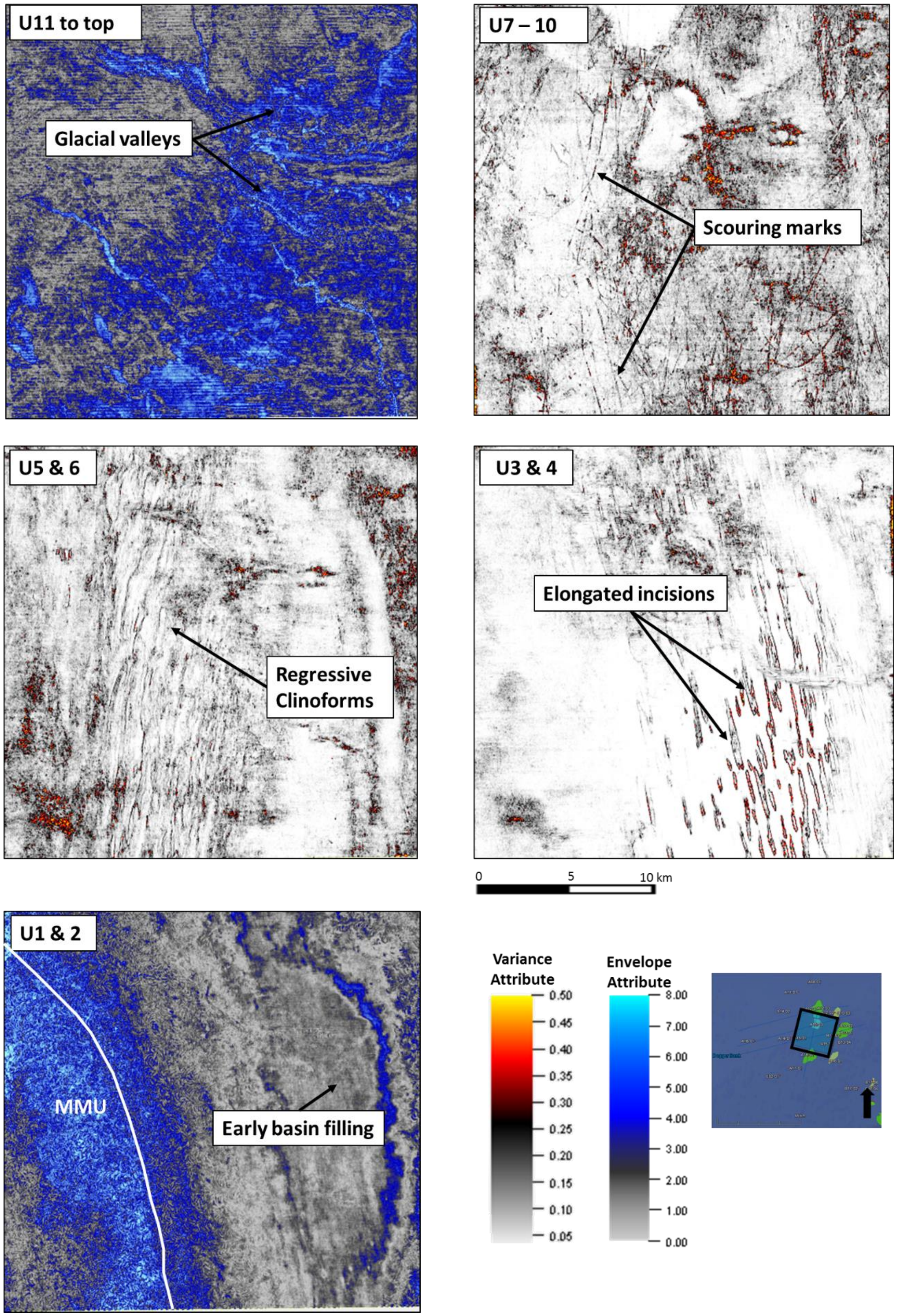

Figure 10: Geological features visible on seismic attributes from seismic 3D survey.

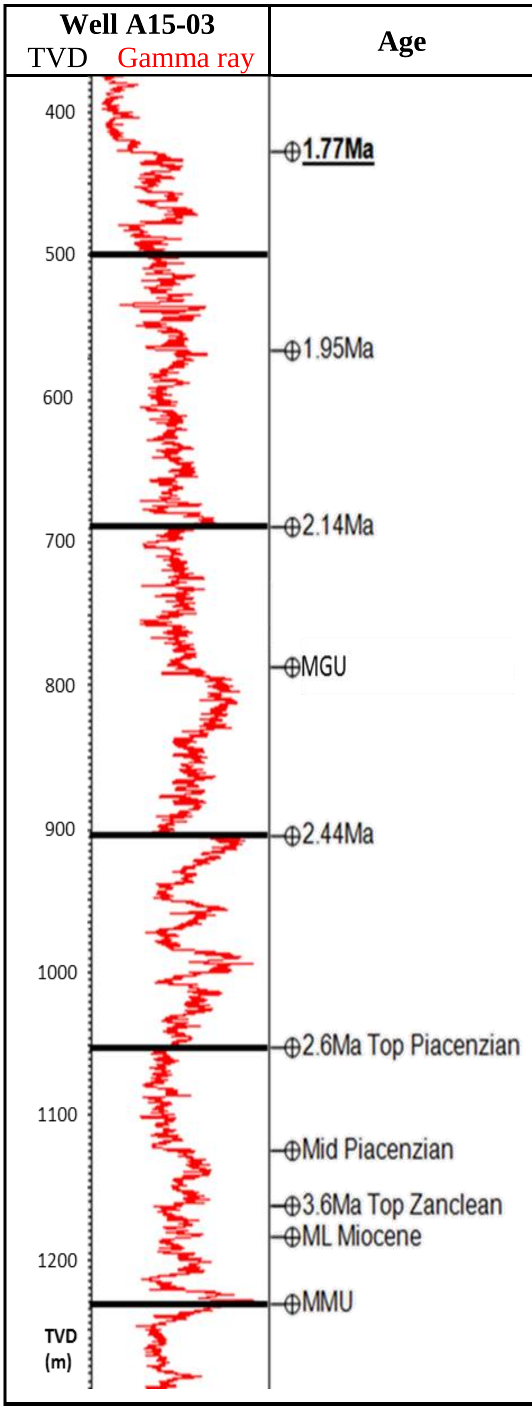

Units of this study	Kuhlmann 2008	Overeem 2001	Paleoenvironment
12 11	13 12	23 20 19 18	Fluvial in nearshore under arctic conditions
10 9 8 7	11 10 9 8	17 16 15 14	Shallow marine with arctic conditions and pulses of warmer conditions
6 5	7 6	13 12 11	Restricted marine changing from warm and humid conditions to cool and stable freshwater
4 3	5	10 9 8	Transitional with alternation between warm and cold intervals and variation in water salinity
2 1	4 3 2 1	7 6 5	Open marine with a relatively deep basin

Figure 11: Paleoenvironmental interpretation of the seismic units based on the paleontological studies by Kuhlmann (2006) and Van Den Belt (2000) with the seismic units equivalents of Overeem (2001) and Kuhlmann (2008).

6. Results

6.1 Sequence Stratigraphy

Both well wireline logs and seismic reflections were used to construct a sequence stratigraphic framework that can be applied for the interval between the MMU and top of the delta (dated to around 1.77Ma). A remarkable change in base level occurred during the MGU, which can be identified both seismically and from wells wireline logs. Units 1-5 remark the major transgression overlaying the MMU, where seismically the units onlap on the unconformity to the west. Judging from the petrophysical properties and cored intervals, those mostly are made of shale and silt with minor coarser grains intervals. Unit 6, which is right above the MGU marks the start of regression, where forced regressive clinoforms deposited in response to the drop in base level (Figure 12). Units above (Unit 7 - 10), are characterized by lower gamma ray that are recognized seismically as packages of prograding wedges. This interpreted coarsening upward succession with the prograding sediments ends at unit 11 with aggredation marked by units 11 & 12, where the basin was already filled.

In Figure 13B, sequence boundaries were picked by identifying the erosional contacts between transgressive system tracts (TST) and both highstand (HST) and falling stage system tracts (FSST), where HST is not clearly recognizable in well logs. Overlaying the erosional contact, a sudden base level fall, which is usually accompanied by forced regression is observed (Catuneau, 2002). The parasequences in Figure 13C are picked by identifying shallowing upward sequences that are separated by maximum flooding surfaces (MFS) (Catuneau, 2006). System tracts were also picked on seismic 2D line AB-91-03 on a regional trend showing the variations of gamma ray in wells and seismic response to base level change moving basinward (Figure 14).

To compare the thickness variation of the units, cross correlation between both seismic lines and wells was made. The dip direction of the data is NE-SW, so most of the thickness changes are observed in the direction of dip. Three main cross sections were constructed for correlation purposes. Two of these are from wells showing both dip/strike directions and the variation of units in them. One seismic cross section is used as guidance to fill the space between the well as seismic provide lateral continuity that wells lack. Seismic 2D line AB-91-03 was used as it crosses wells A15-03 and A16-01, so better correlation between seismic traces and wells petrophysical logs could be used to estimate units' intervals and corresponding signatures.

The major observation is the onlapping of the units on the MMU as we move to the SW. Most of the lower units are cut by the unconformity, which made them not traceable on well logs. It's also notable that the thickness of the units between 1.77- 2.14 Ma (units 7-12 in this study) increase dramatically in the same direction (Figure 15 & Figure 16). The NNW- SSE well cross section (Figure 17) show very little variation in thickness and that's due to it being strike oriented. The major thickness increase is in well B17-05 and the picks couldn't be verified from seismic but were adopted from the study by Kuhlmann (2008).

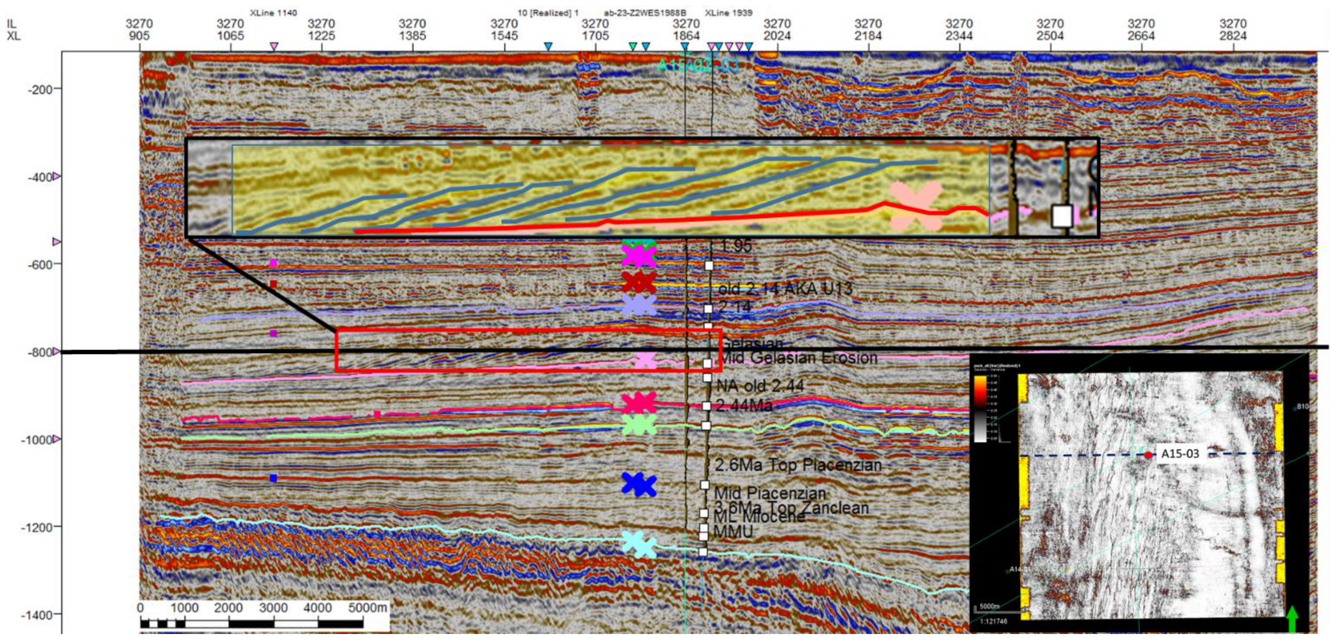

Figure 12: Regressive clinoforms above the MGU with a variance seismic attribute time slice at -800ms on inline 3270.

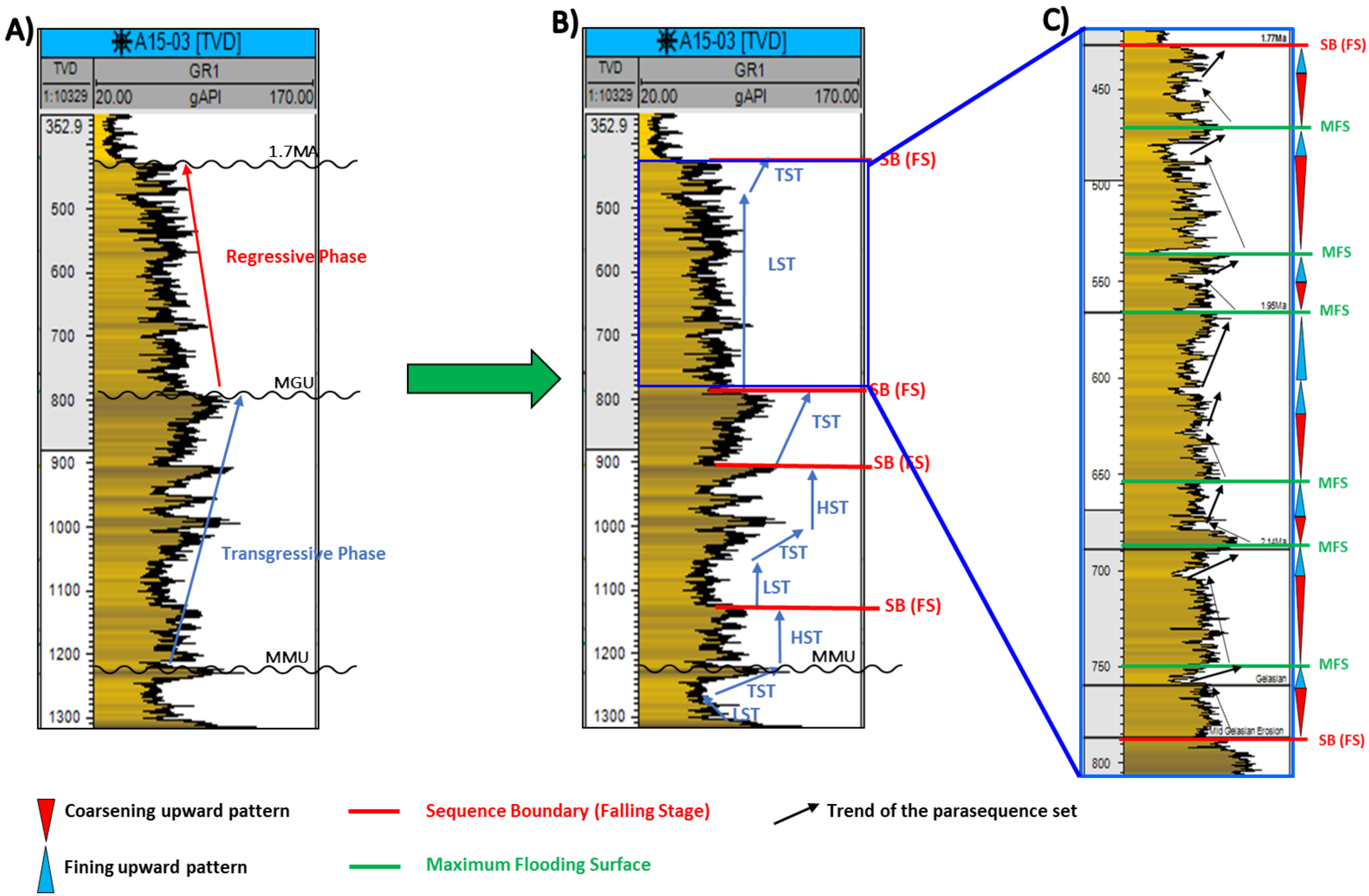

Figure 13: A) A generalized base level response for the shallow section in well A15-03. B) Reconstruction of system tracts of the same interval. C) sea level fluctuation on the MGU-1.7MA.

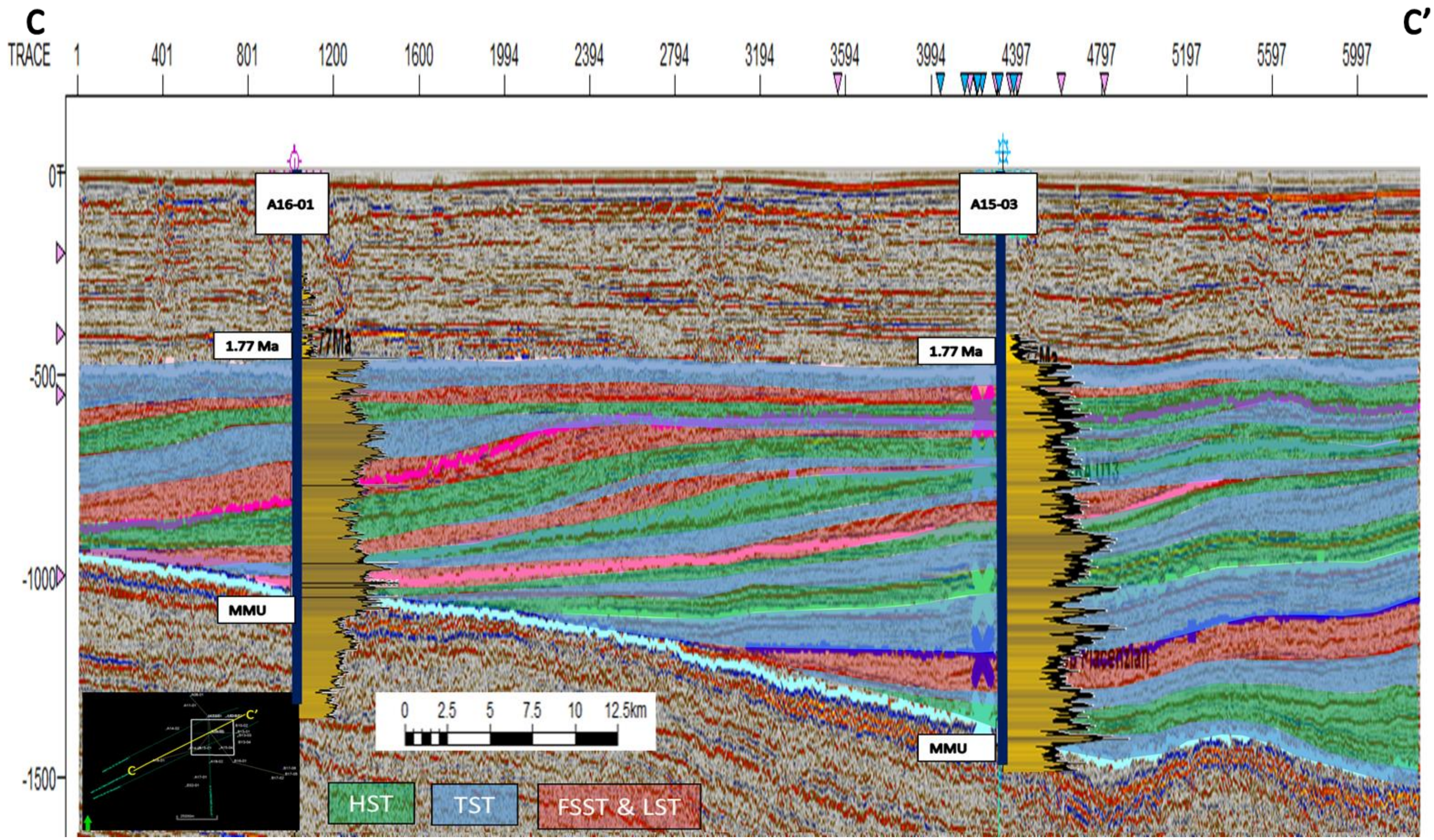

Figure 14: Base level variation and system tracts picking on regional seismic 2D line AB-91-03.

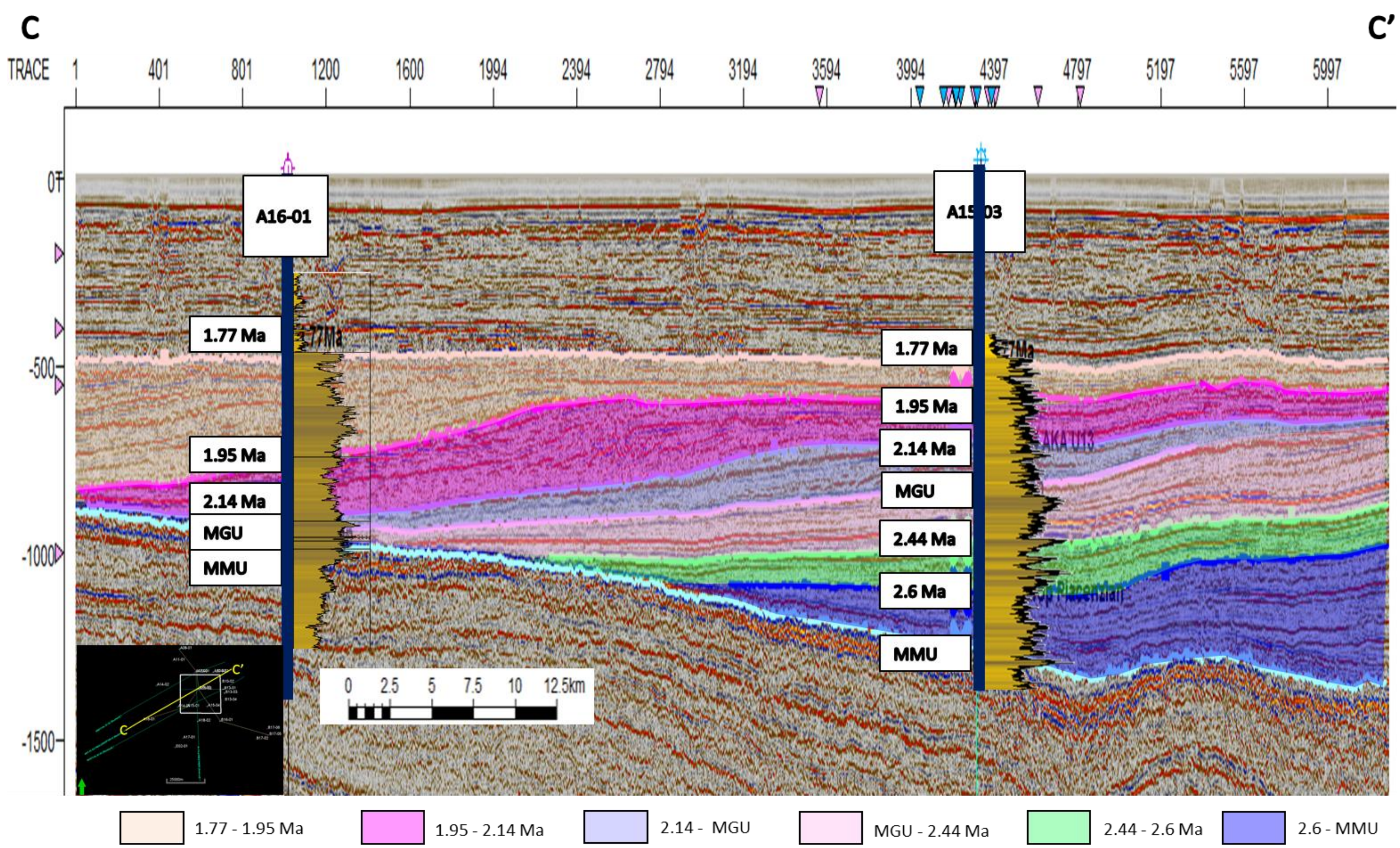

Figure 15: Thickness variations of the age controlled seismic units in seismic 2D line AB-91-03 passing both wells A16-01 and A15-03.

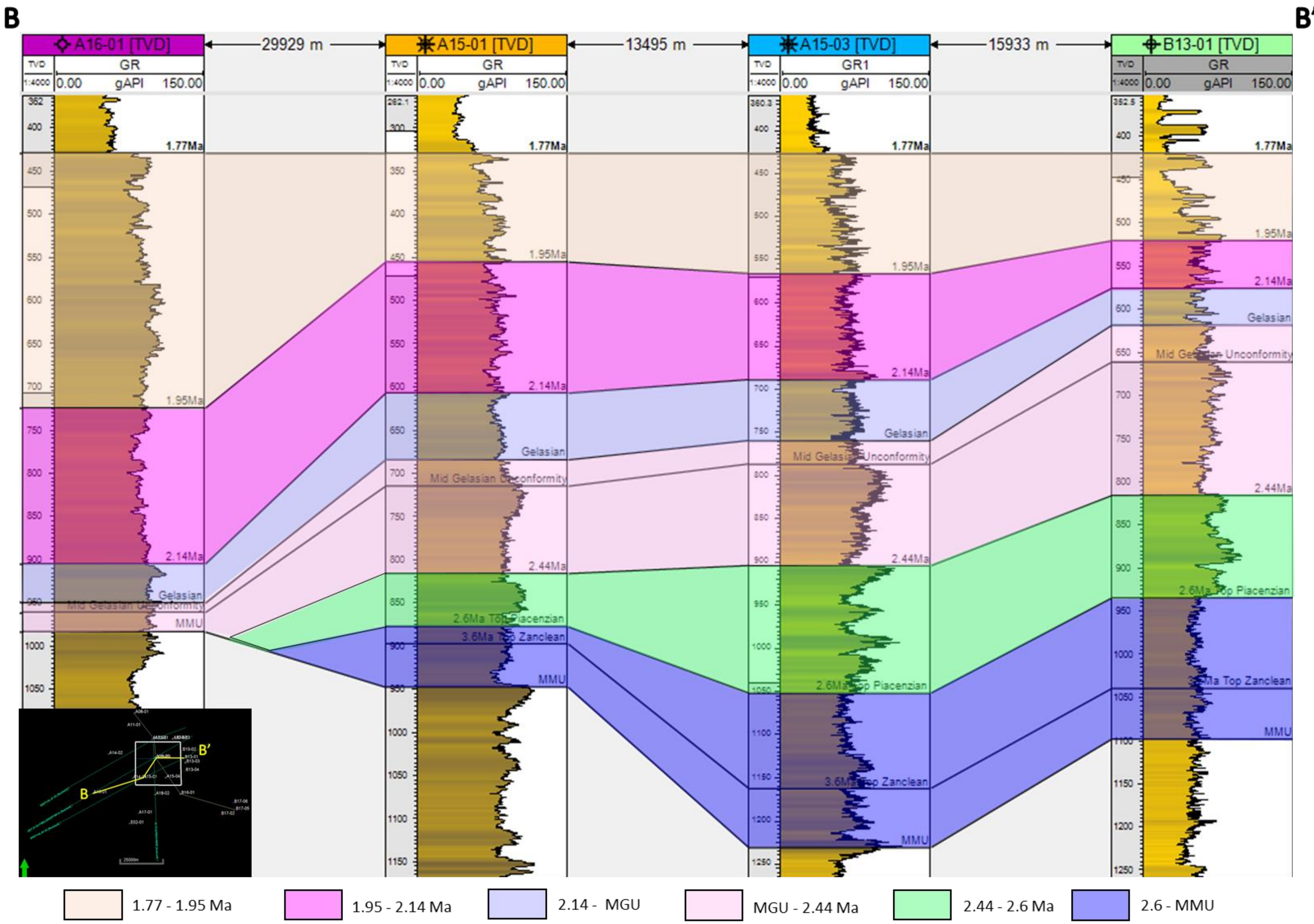

Figure 16: A NE – SW wells cross section showing the variation of thickness in a depositional dip direction.

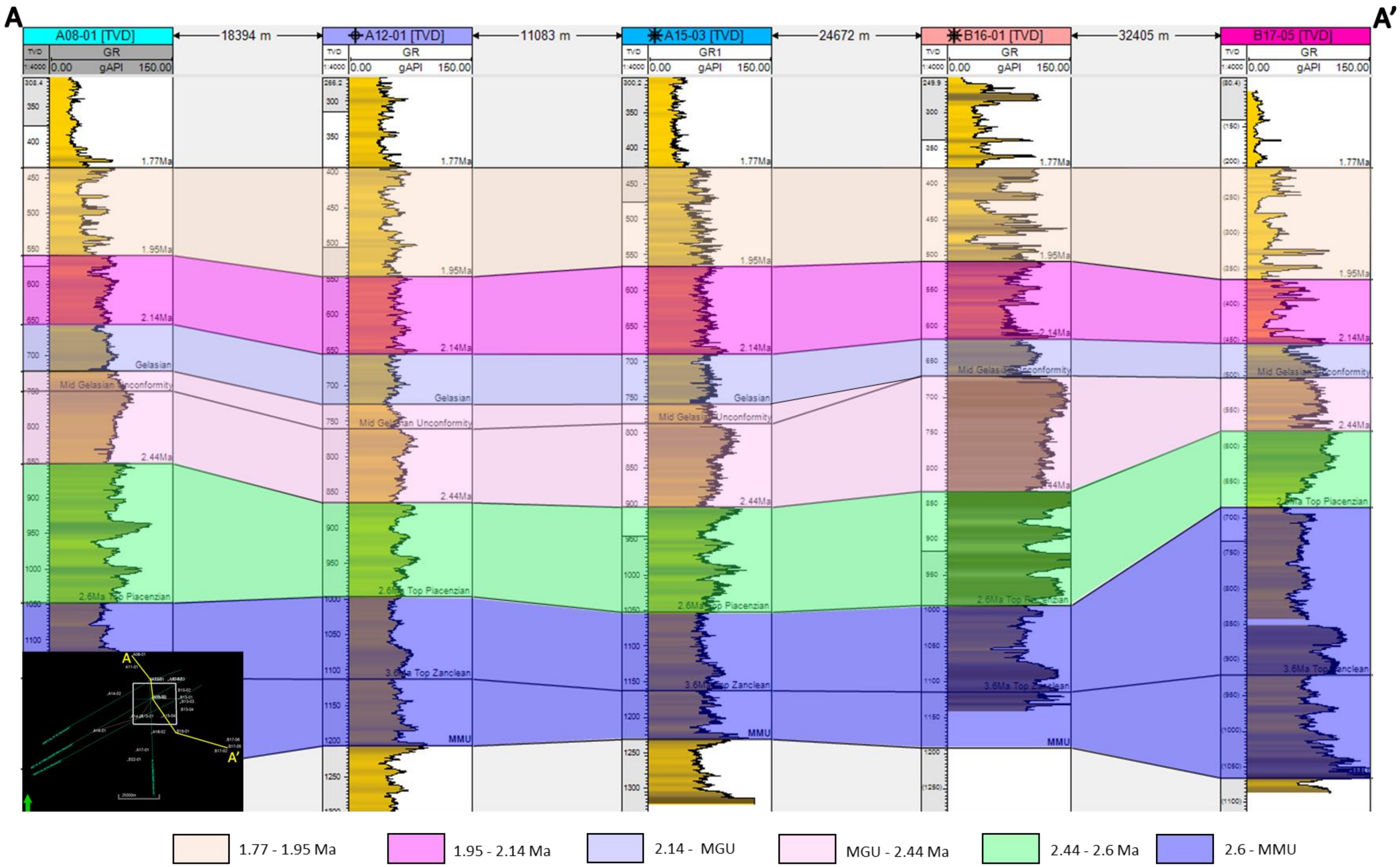

Figure 17: A NNW – SSE wells cross section showing the variation in thickness in a strike direction.

6.2 Rate of Sedimentation and Delta Horizontal Shift

For the shallow section of the North Sea, climate change and the alternation between cool and warm periods have a direct impact on sedimentation. Glaciation triggers erosion and on the warmer periods the transportation of the sediment is enhanced by deglaciation, which is observed in the sedimentation rate (Kuhlmann, 2008). Ten Veen (2013) suggests that cooler periods have very fine materials depositing, while the warmer ones have coarser grains. This could apply especially for sea floor as the wave energy is lower during cooler periods (Stuart, 2012). Sediment volumes of this study uses the ones calculated by Overeem (2001). Both Kuhlmann (2008) and Overeem (2001) used the same sediment volumes to calculate the sedimentation rate and the outcome of both studies is different. The reason behind the variation in the results is the difference in the assigned absolute and relative ages of the seismic units, which gives different time duration for the deposition of each unit. Overeem only used an exponential relation starting at 10.7Ma for the first seismic unit to predict the time each subsequent unit took to deposit. In the study done by Kuhlmann (2008), more age control was implemented and resulted in a more detailed estimation of the sedimentation rate. Three absolute ages were used, which are 3.6Ma, 2.6Ma and 1.95Ma. The age of the units between these three controlling points was determined based on a liner distribution, so a constant time increment was given between each controlling point and the following one (Figure 18).

Prior to both studies, age estimation based on well A15-03 was established in 1999 by R. Verreussel, who did the study on the palynomorph, and H. Jansen, who carried out the study on the foraminifera. The major difference between the biostratigraphic outcome of the study and the results of Kuhlmann (2006) is in the interval between 550 – 900 m. According to Verreussel & Jansen, the time it took to deposit the interval is 0.25Ma. The study by Kuhlmann suggests at least 0.50Ma for the same interval. In terms of sedimentation rate, which is calculated from the volume of sediment and accumulation time, following the study by Verreussel & Jansen gives an anomaly in the rate due to the short duration allocated (Figure 19 & Figure 20C).

Kuhlmann also tried to estimate some intermediate age controls between the three absolute ages used in the linear distribution. Applying those extra control points changes the sediment rate dramatically as the durations it took for the units to deposit decrease (Figure 19 &Figure 20B).

All the plots have similar trends. The sedimentation rate varies in magnitude, but overall moves from low rate to high reaching the maximum in seismic units 4-6 (corresponds to units 5-7 in the study by Kuhlmann, 2008) then decrease again. The reasoning behind such peak in sedimentation rate is attributed to enhanced cooling that triggered more erosion, and that isn't just a trend which is observed locally but even on a global scale other regions recorded such increase for the same period of time (Kuhlmann, 2008). This study favors the extended ages estimated by Kuhlmann as more controlling points are added between the three ages used in her study, which is based on paleontological observations of well A15-03. While linear distribution gives smoother increase in sediment rate, the approach assumes constant increment when some extra controls could be used. Using the age control by Verreussel & Jansen is the least likely since a dramatic jump in sediment rate from 2.0 – 2.1 Ma lacks evidence and cannot be linked to any abrupt change that can cause such an anomaly at the time.

The progradation distance is measured by locating shelf breaks of the delta in the seismic units, then measure the distance between each shelf break and the corresponding younger one of the next unit. These measurements were done on the three dip oriented (NE-SW) seismic 2D lines. Instead of taking the average a range based on the three values for each unit's progradation distance is given in Figure 21. It is worth noting that neither the volume nor the duration of the units is constant so the distance is only an indication of the progradation recorded in time and a high value doesn't necessarily indicate a sudden increase but time between the units should be noted when comparing different units. We can observe that the progradation distance of units 6&7 is the highest and that align with the sedimentation rates (Figure 20) while both measure different parameters (progradation distance and volume of sediment deposited in time). As the basin was already filled, having a directly proportional relation between sediment rate and the progradation distance is expected as the supplied sediment should exceed the accommodation space available. For the younger units, the units look thick but a decrease in the sedimentation rate and progradation distance is observed and that could be attributed to local buildups rather than lateral extent. From unit 11 upward we can only observe aggredational character as the basin was already filled (Kuhlmann, 2008).

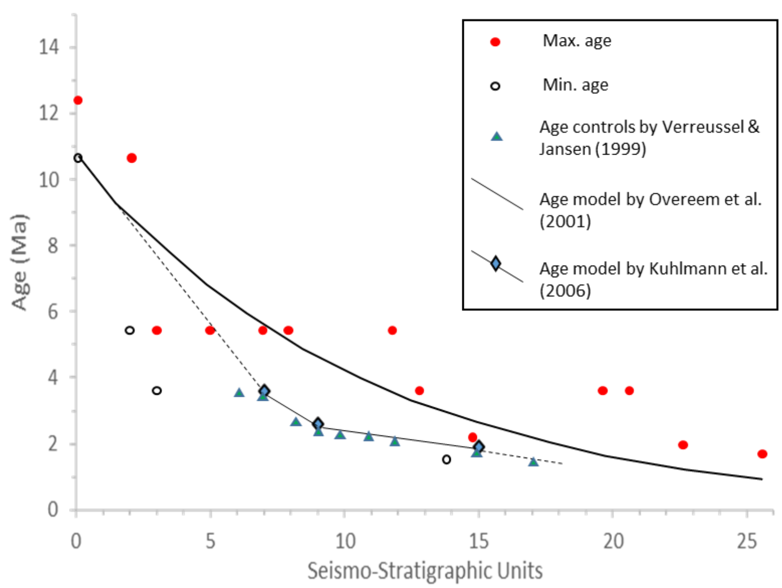

Figure 18: Age comparison between the three models represented by showing the seismic units of Overeem (2001).

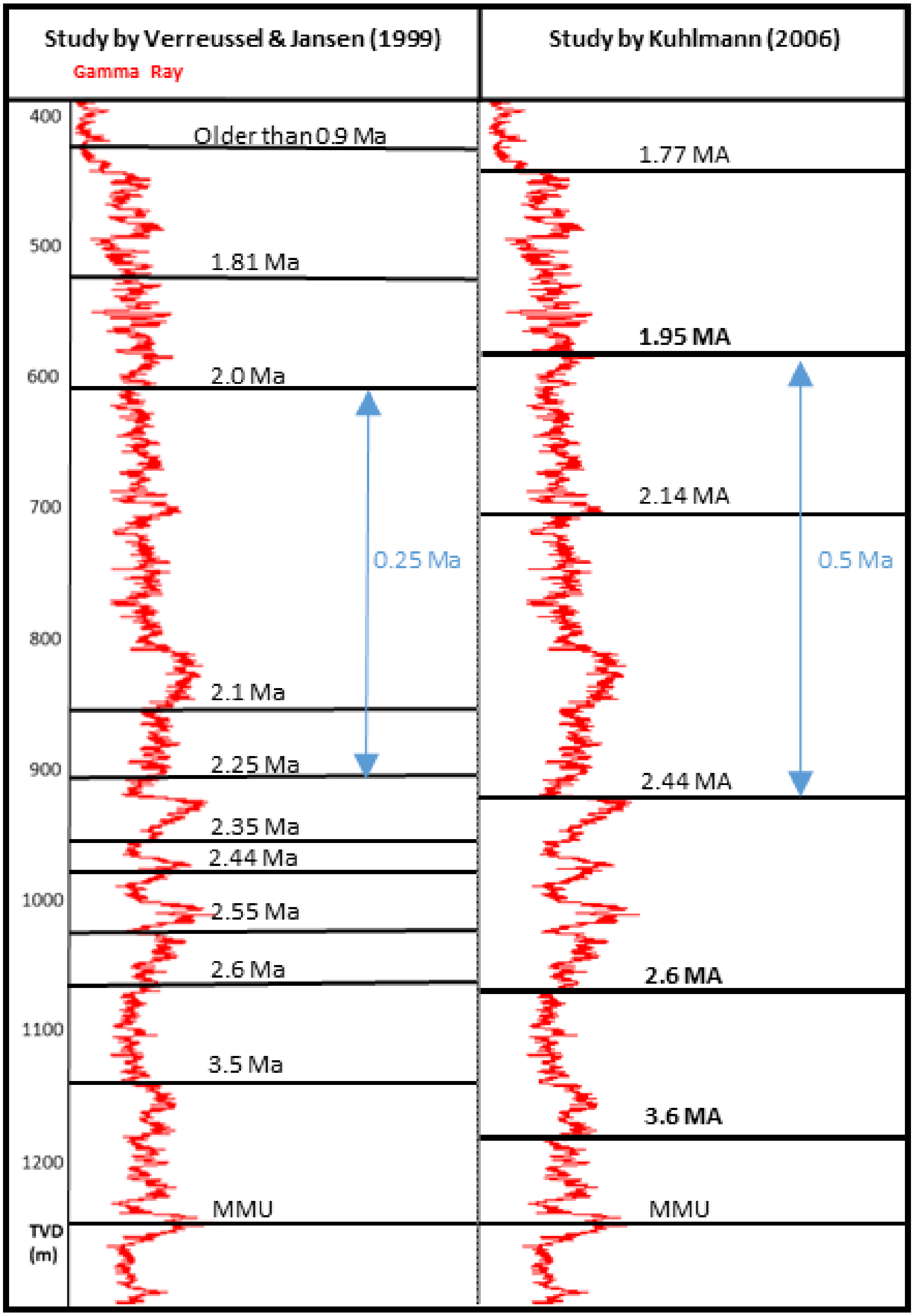

Figure 19: Well A15-03 showing gamma ray variation with depth and the age estimations of Verreussel & Jansen and Kuhlmann.

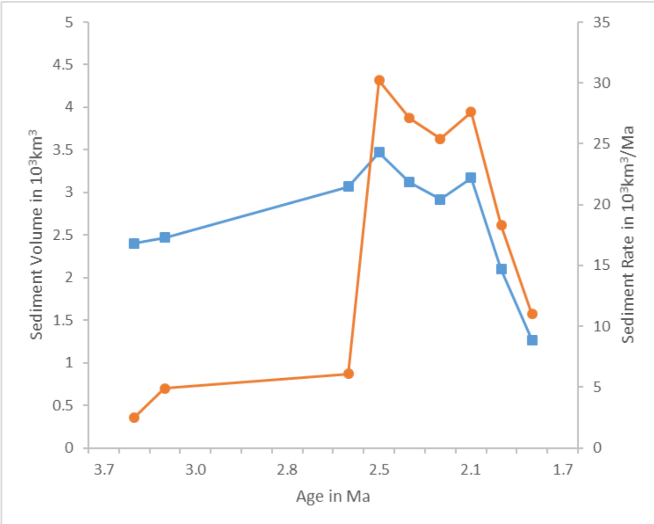

A) Plot based on Kuhlmann linear increment of points 3.6Ma, 2.6Ma and 1.9Ma.

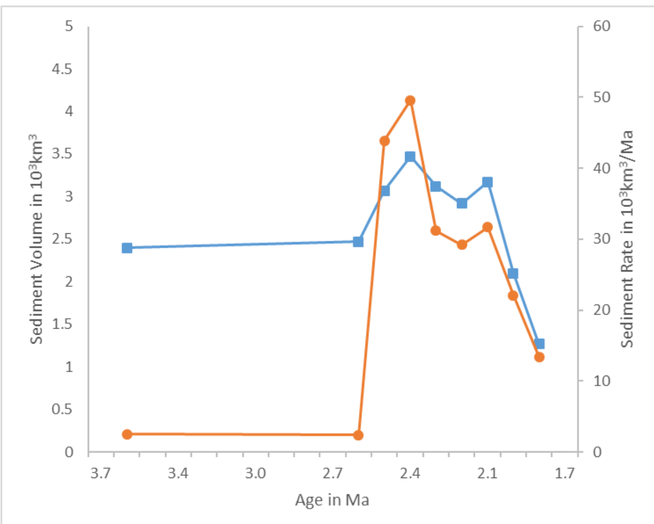

B) Plot based on Kuhlmann extended estimation of age controls.

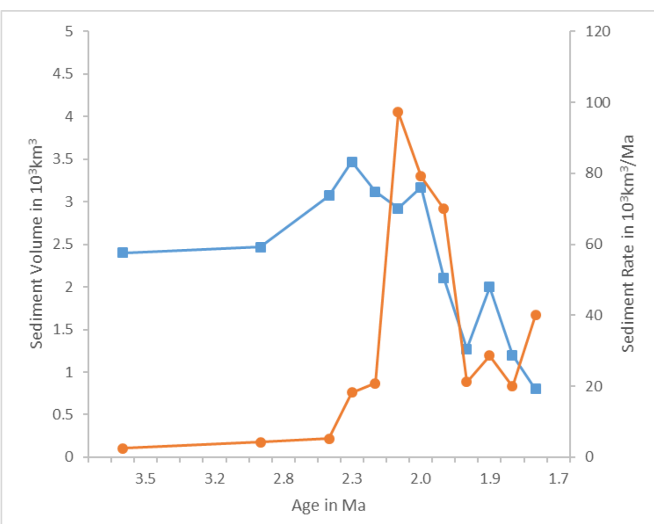

C) Plot based on age controls by Verreussel & Jansen.

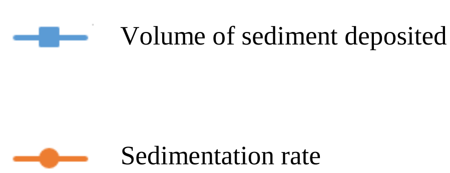

Figure 20: Different Sediment volumes/rates schemes based on absolute age predictions by Kuhlmann (2006/2008) and Verreussel & Jansen (1999).

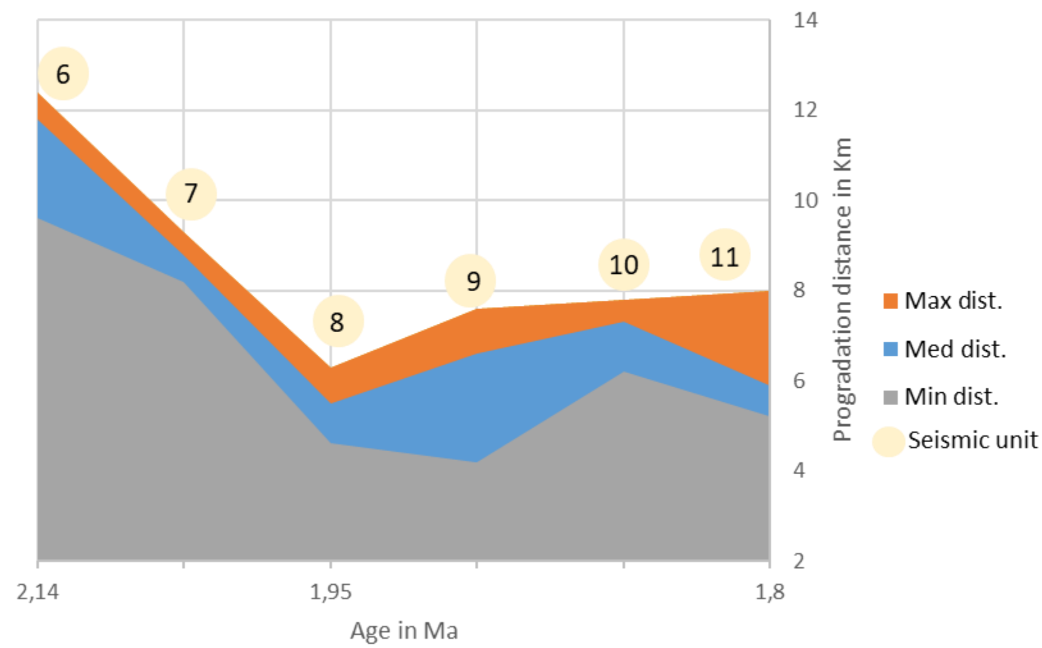

Figure 21: Progradation distance in time plotted using the three 2D lines (Sns-87-03, ABT-91-03 & Sns-87-02).

6.3 Reservoir Characteristics

In this study a total of 20 wells were used to identify the characteristics of the shallow section (< 1km) of the North Sea Basin. Seven of these wells have core descriptions and plugs analysis including porosity, permeability and density. Lithofacies from both shallow marine and deeper marine are present (Figure 4). Lower section consists of alternations between silty turbidite deposits and claystones, while the upper one is an alternation of shoreface sands, clays and silts (Van Den Belt, 2000) (Figure 5).

While the coring measurements vary in depth and age, majority were taken from the zones in which reservoir potential was expected, which means whereas these measurements are representative of the reservoir, the other un-targeted zones could be completely different. The two core measurements which this study focuses on are porosity, and how it varies in depth for the shallow section, and permeability and whether or not it has a relation with porosity.

Despite the change in depth for the coring intervals, porosity of the reservoir zones varies from 25-45% (Figure 6). While other parameters are used to determine what value of porosity is considered effective for production (e.g. saturation, volume of shale and pressure), by industry standards for producing reservoirs the porosity exceeds the cutoff not just for gas, which can work with lower parameters, but even oil (Mahbaz, 2011). The other key parameter, which porosity is entirely used for is permeability. In Figure 7, an exponential trend line is added and it shows a direct relation between the porosity and permeability of the scattered points. The equation in which permeability can be predicted when knowing the porosity is:

$$\textbf{Permeability} = \mathbf{5E\text{-}6\ e^{45.808 \times Porosity}}$$

Generally, the permeability range from less than 0.5md all the way to 4600 md. It is worth noting that although the graph shows a well-established trend, same porosity measurement could have a wide range of permeability values (e.g. in Figure 7, 30% porosity corresponds to 0.2 – 700md). While the relation between porosity and permeability is complex, some variation in the cores is attributed to intense burrowing with clay filling that can locally degrade the reservoir quality (Van Den Belt, 2000).

6.4 Shallow Gas Potential

To assess where higher quantities of gas are present, tracing the gas to its origin and understanding how it migrated to the reservoirs can aid in predicting which locations may host larger accumulations.

Two sourcing origins could vindicate the occurrence of these gas accumulations, which is either being sourced from a biogenic or thermogenic origin (Schroot, 2003). Both origins have organic materials, however, biogenic process is based on bacterial activities to convert organic matter into gas, while the thermogenic origin is based on burial of the source rock being pressure and temperature dependent to generate gas (Schroot, 2003). Although the biogenic origin is favored for shallow gases, as thermogenic gas window is quite deep and requires long distance migration, having the producing fields only above the gas chimneys or close to them suggests a deeper source rock (Connolly, 2015). Those gas chimneys are generally above the Zechstein salt domes, which might suggest another element. Normal faults and fractures are associated with these salt domes which create migration paths to the reservoirs (Schroot, 2005). This doesn’t only provide gas migration of deeper source rocks but could allow any shallow biogenic gas to be transported to the reservoirs. Knowing the main origin requires geochemical evaluation of the carbon and hydrogen isotopes, which in this case still can be altered by bacterial activities (Schroot, 2003). Presence of gas chimneys was verified in all the discoveries within this study’s area, and those are the discoveries in blocks A12, A15, A18 and B13 (Figure 22). Gas chimneys are identified seismically by push down features and velocity disturbance vertically that give a column of attenuated amplitudes (Marzec et al., 2016).

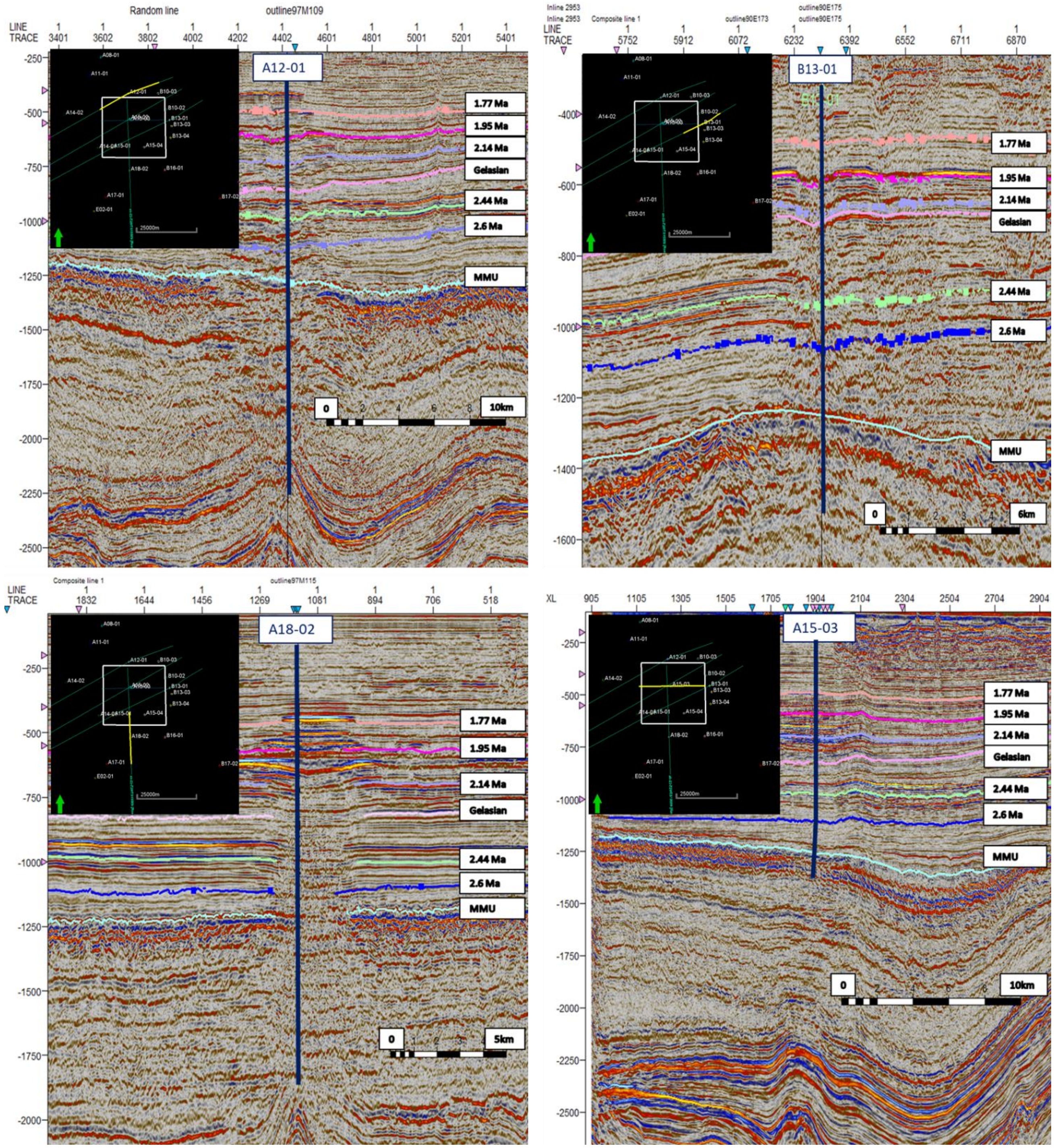

Figure 22: Presence of gas chimneys below the discovered fields in the study area.

7. Integration of Study Results and 3D Modelling

Study results were integrated to construct a 3D model which shows the extent and properties of the mapped seismic units. Components of the model are seismic interpretation (structural maps, velocity models and attributes), stratigraphic interpretation (litho, sequence and chrono) and petrophysical interpretation (correlation of wireline logs, core analysis) (Figure 23). At well locations, interpretation of lithology was constructed from cutting samples that are provided in well composite logs (from nlog.nl). Extra methodologies were used in this section to populate the model with lithologies and petrophysical properties.

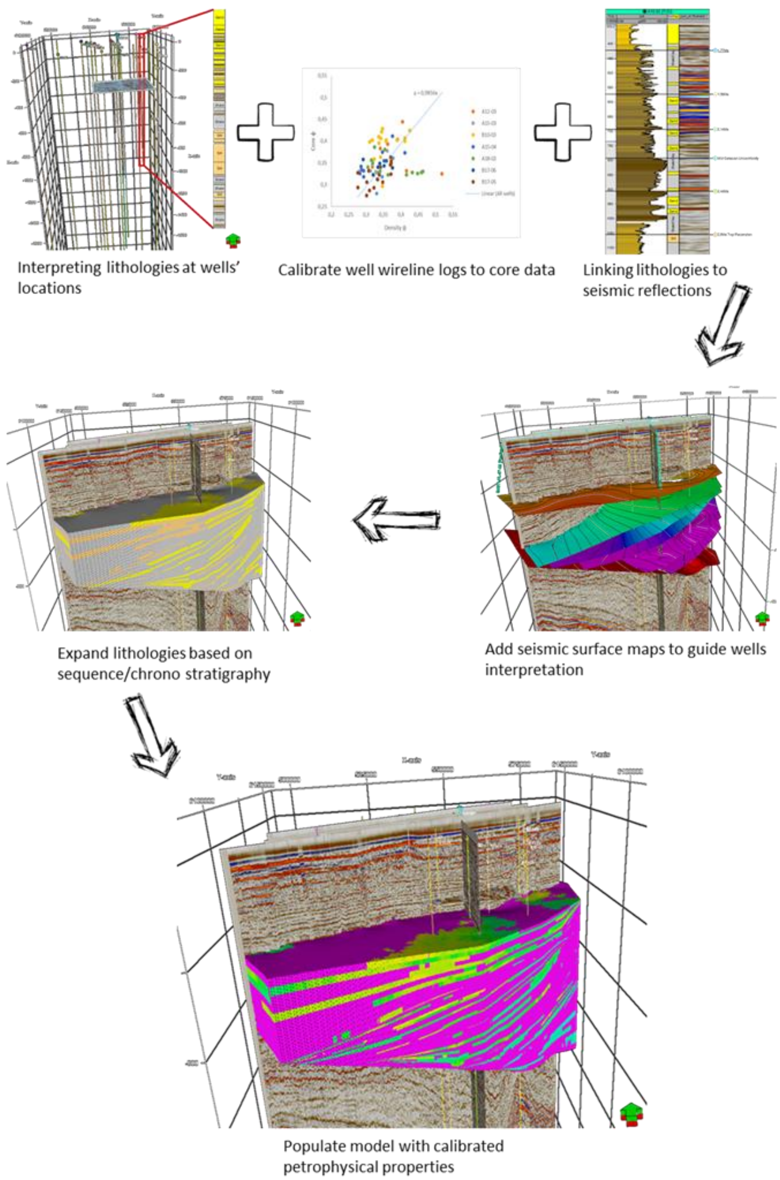

Figure 23: 3D modeling workflow and data integration.

To extrapolate the lithologies, seismic data influence on the trend was implemented by creating velocity models of each unit. This was achieved by calculating the interval velocities given by Dix formula which provides the difference in velocities between the top and bottom layers.

$$V_{Int} = \sqrt{\frac{{V^2}_2 t_2 - {V^2}_1 t_1}{t_2 - t_1}}$$

Where, V_{Int} is interval velocity, V_2 is the velocity of the base layer, V_1 is velocity of top layer, t_2 and t_1 are reflection arrival time of bottom and top layers respectively.

When the velocity model was applied, amplitude ranges were automatically picked for each lithology of the wells on seismic data and those were used as guide to the trend for the extent of the lithologies.

Another methodology was implemented to calibrate core porosities to wireline logs using both density porosity and neutron porosity (equations from Anovitz & Cole, 2015), to identify which gives better estimation of the un-cored zones' porosities.

Two equation were used; one is to determine porosity from density which is:

$$\Phi_{den} = \frac{\rho_{ma} - \rho_b}{\rho_{ma} - \rho_f}$$

Where, Φ_{den} is density porosity, ρ_{ma} is matrix density, ρ_b is bulk density, ρ_f is fluid density. As two different reservoir lithologies were mapped, different ρ_{ma} were used in the calculation. ρ_{sand}= 2.655 (g/cm3) and ρ_{silt}= 2.798 (g/cm3) (Abdulkadir, 2016). Likewise, ρ_f is different for water and methane as 1 (g/cm3) and 0.668 (g/cm3) respectively. Well test results and production data (Table 3 & Table 4) were used as a guide to when methane is to be used instead of water for the fluid fill.

To average both density porosity and neutron porosity:

$$\Phi_{ave} = \left(\frac{{\Phi_N}^2 + {\Phi_{den}}^2}{2}\right)^{\frac{1}{2}}$$

Where, Φ_{ave} is averaged porosity, Φ_N is neutron porosity.

Results of both porosities were plotted against core porosities and linear relations were established (Figure 24 & Figure 25). Of the two calculated porosities, the density porosity is the closest to mimic the porosity obtained from the cores, having around 98% match, so it was used to generate a porosity log for the lithology zones. Porosity was assumed to be zero in the layers which were labelled in cutting samples as shale or clay since they aren't reservoir zones. Permeability was calculated using the relation in Figure 7 at well locations and then extrapolated to cover the porous reservoir layers. For gridding the calibrated logs, Sequential Gaussian Simulation (SGS) was used, which simulates the subsequent grid points from the observed data using a Gaussian (normal) distribution of a random function model (Delbari, 2009) while still can be guided by secondary data like seismic amplitudes, lithology grids or production data.

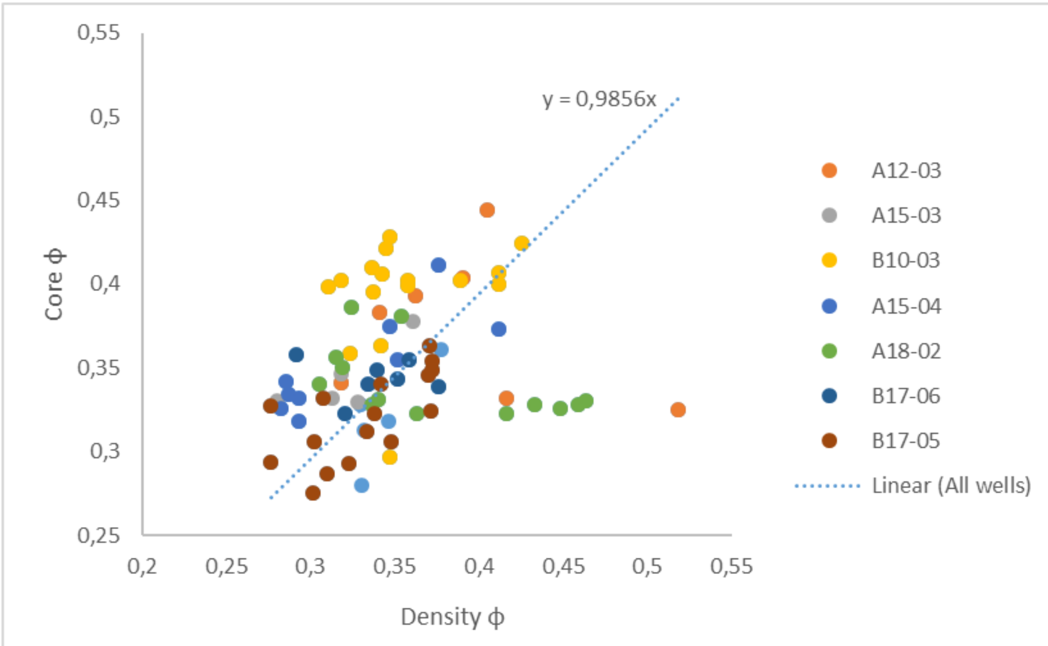

Figure 24: Relation between core porosity and density porosity.

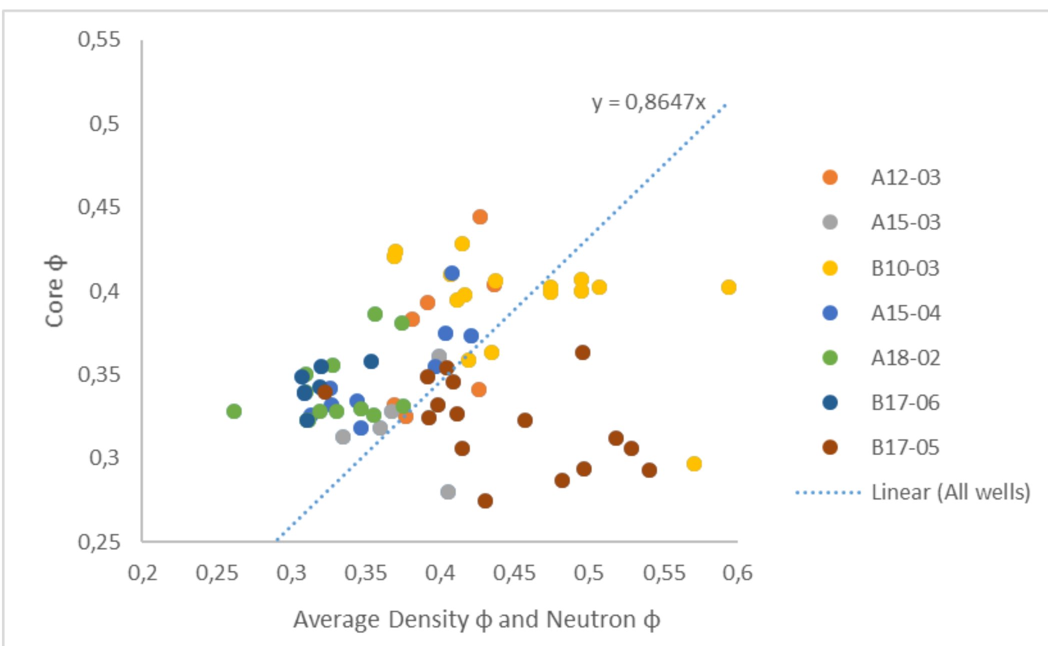

Figure 25: Relation between core porosity and averaged porosity.

8. Discussion

While part of the results in this study confirms previous ones done in similar blocks, some results vary and are supported with different point of view. Mostly two discussion topics are being covered in details. One is the depositional origin of units 3 & 4 and the elongated structures present in them. The second topic is the gas in the shallow section of the North Sea and what elements should be confirmed when exploring for gas.

8.1 Depositional Settings of Units 3 & 4

As observed in Figure 10, some elongated features are dominating the time slice of units 3 and 4. Those features where described by Kuhlmann (2008) and Stuart (2012) as elongated incisions that are caused by strong sea bottom currents. Kuhlmann stated that those are a prove of alternation between cold and warm periods, while cold periods grain sizes are very fine and warmer periods are slightly coarser (mostly silt) with those incisions occurring due to the higher energy of bottom currents. The incisions as discussed in both studies could be attributed to either one of two depositional models. One is, along the slope bottom currents incising the deposited very fine grains and another is caused by currents down slope of the prograding wedge. Kuhlmann supports the first model as the structures imaged seismically are parallel to the slope and not downslope and interprets the current direction of incision to be from North to South. Stuart describes the features as incisions caused by strong bottom currents cutting into the sands and predicts incisions to be of the opposite direction to Kuhlmann (from the South not the North) based on the shape of the elongated incisions which is narrowing to the North.

A study by Seranne (2000) suggests another model of such elongated featrues that doesn't fundamentally provision erosion. While circulation of bottom currents still is the main cause of the structures, their affect is somehow different. Sea bottom currents as described by Seranne can work to prevent sedimentation from the hemipelagic suspension settlings. This means, that the currents are syn-depositional rather than post-depositional, in the sense that while settlings of the very fine particles occur, at sea bottom where the currents are stronger, no deposition of sediment happens. With time the currents take preferred routs and that causes elongated incision-like structures to appear. It is worth mentioning that while this doesn't fully ignore the possibility of some erosion on the flanks, caused by the instable energy of the sea bottom currents, erosion isn't the main mechanism for the features.

In this study the proposed model by Stuart (2012) is favored based on three reasons. Firstly, the structures aren't downslope as they are parallel to the delta front (Figure 26). Secondly the direction of the incision is from South to North as these incisions are more dominant in the South and narrowing to the North, which could indicate a loss of energy of the bottom currents moving North. Lastly, erosional contacts are visible in the cross section in Figure 26 on the bottom layer and turbdites are found within the same stratigraphic interval in well A15-03 (Van Den Belt, 2000), which could also support erosion.

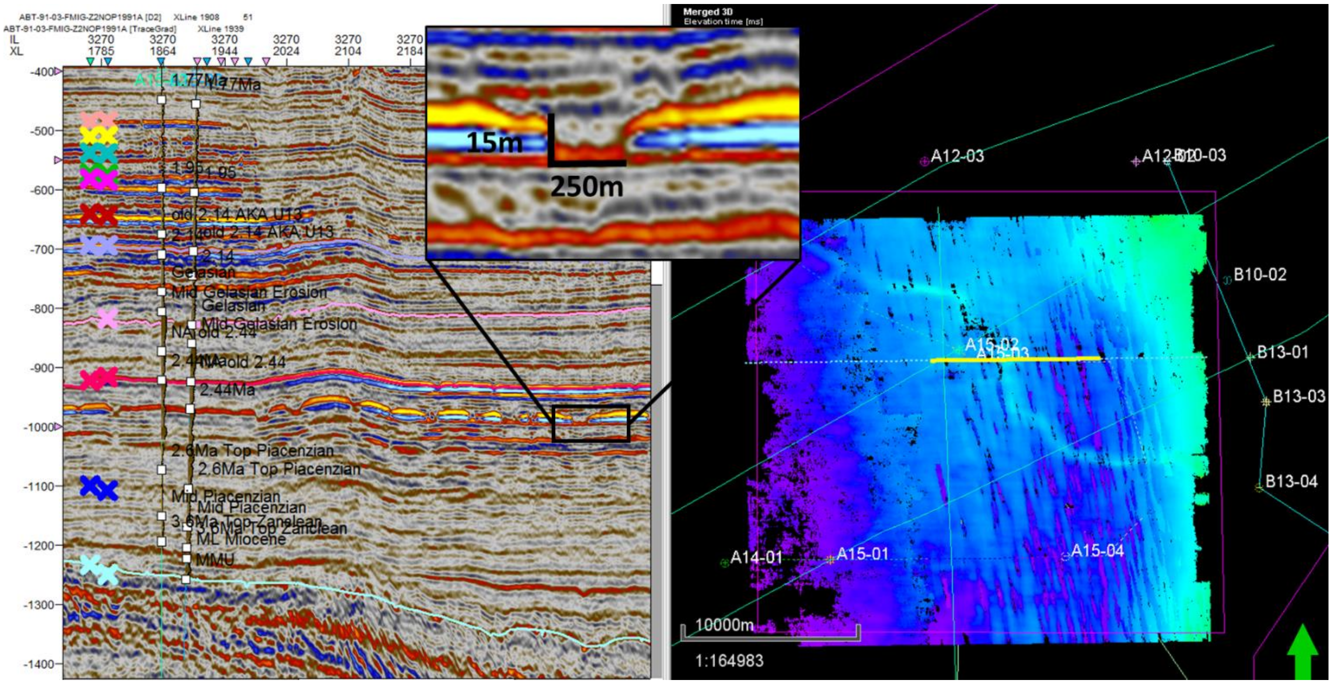

Figure 26: Elongated incisions caused by sea bottom currents in units 3 & 4.

8.2 Shallow Gas Potential and Main Controls on Further Discoveries

Gas accumulations in the shallow section are already proved in seven fields in the A and B blocks, in which three are producing, in addition to wells in other locations within the North Sea Basin that proved hydrocarbon shows through either production tests or high mudgas readings (Table 3 & Table 4). As observed from the locations of the discoveries, the gas accumulations of the North Sea shallow sediments are all in the Northern blocks and the reason behind such concentration of discoveries isn't fully understood. From the wells'shows in Table 3 and by looking at the wireline logs and core data, the presence of reservoir and seal rock isn't the main factor that caused gas accumulations not to be present. Some wells still have reservoir zones with high porosity and permeability (Figure 7) that are overlaid by shale layers and yet only traces of gas were observed. In fact, historically, the shallow section is known to be gas bearing and was considered hazardous as it is highly pressured in some locations (Van Den Belt, 2000). To overcome the problem, rising the mudweight and drilling overbalanced was the common technique to avoid blowouts (Jilani, 2002) when targeting deeper Paleozoic and Mesozoic reservoirs.

As this study only contains seismic data around the producing and undeveloped fields, very little comparison to the other unsuccessful locations can be made, nevertheless, success factors can be assessed.

Three main features of the producing fields can be correlated. The first factor is the sedimentological facies and the reservoir/seal properties. The second factor is related to charge and what sort of source is feeding the reservoirs. The last factor is the trapping mechanism. This study suggests that wherever, reservoirs with clay seals are present above gas chimneys, discoveries were made.

8. 2.1 Factor one: Sedimentological facies of the reservoir and seal rocks

The nature of the reservoir and seal is a very important aspect of the hydrocarbon potential. Interbedded very fine grains (shales) and coarser grains (sands and silts) are main seal and host of the gas. Those are attributed to the alternation between warm and cool periods in which different lithologies can deposit. Grainy rocks are correlated to warmer climate and very fine grains are of the colder one (Kuhlmann, 2008). Such observation can be made either seismically, looking at seismic attributes, or petrophysically, by interpreting well wireline logs.

Seismically, lithological variation and change in porosity can be inferred by studying seismic attributes (once a 3D coverage of different parts is available) as seismic velocities are sensitive to change in density of the layers, which changes as lithology or porosity vary. Change in contrast of impedance and tuning in amplitude can mark the switch from high to lower density rock (Subrahmanyam, 2008).

Petrophysically, wireline logs can predict grain size distribution especially when calibrated to core data (Glover, 2000). The most common wireline logs for grain size prediction are gamma ray, neutron porosity and density. Neutron porosity and density are mainly used to identify lithology and porosity, while gamma is generally used to identify clay and differentiate between effective and non-effective porosity (Fristad, 2012). As some cores are available and interpreted in terms of depositional environment, direct calibration to core data can lead to a good estimation of where similar facies are present based on their wireline logs response (Yan, 2001).

Once the location of those are identified then the first element of the producing fields is granted, which is porous clastic reservoir overlaid by shales and clays which serve as a seal rock. What remains of the factors is the filling with hydrocarbon and that can only be predicted by knowing the nature of the source rock and how the hydrocarbon migrated to the traps.

8. 2.2 Factor two: Origin of gas and migration paths

The type of hydrocarbon in the shallow section is gas (methane). The sourcing of gas in shallow sections is controversial as gas source rocks are deeply buried to be in the gas zone. As discussed previously, two main sources of gas are normally attributed to such discoveries. Either from a biogenic origin, which doesn’t require deep burial but can be produce gas, when sufficient organic matter is present, by bacteria to generate gas (Yuwono, 2012). The other possibility is deeper source rocks, which generated gas. Those are still likely but require long distance migration paths to charge the shallow reservoirs. In some cases, the shallow gas is a combination of both and differentiating the origin is proved to be diffecult when both actually contribute as bacteria can severely alter the composition of gas (Connolly, 2015).

Schroot (2003) carried a geochemical study of hydrocarbon fingerprints using old data and some new pockmarks to determine the origin of the gas. While most of the studies support a thermogenic origin, that comes from Mesozoic oil source rocks and Paleozoic (Carboniferous) source rocks, biogenic gas is still detected.

In this study, the thermogenic origin of the methane is the most supported one, while not denying some mixture with biogenic gases. The reason behind this interpretation is the presence of gas chimneys below the discoveries or very close to them (Figure 22). If the gas was only derived from biogenic activities, then some areas absent of gas chimneys will still contain shallow accumulations, and that's not observed. In addition, the reason behind not excluding the presence of biogenic gas even when gas chimneys are behind the methane is that the created fractures and faults by the salt domes, that the deeply sourced gas transported through (Connolly, 2015) can still be used as migration paths by the biogenetic gas. So, not only do the chimneys feed the reservoirs but could also be of significance for the gas with a biogenic origin by granting the presence of migration pathways.

8. 2.3 Factor three: Presence of a trapping mechanism

In all of the producing fields, anticlinal configuration of the structure is present, which is observed from seismic data. The main derive of these structures are the presence of the Zechstein salt domes below. These paleo highs contribute to both the presence of gas chimneys (migration paths) and forming anticlines (trapping mechanism). An additional aspect to consider when new exploration locations are chosen, is whether or not gas clouds are visible in seismic above the targeted reservoir. Gas clouds, when present above the targeted reservoir, indicate leakage of gas and that decrease the seal integrity (Connolly, 2015).

Conclusion

- Data from high resolution seismic 3D data and 2D lines were interpreted, where 12 seismic units were mapped based on their lateral continuity and contrast in impedance. Units 1 – 5 are below the Unconformity that occurred during the Mid-Gelasian (MGU) and are marked by transgressive sequences representing the basin fill following the MMU. Units 6 – 11 is represented by delta prograding wedges dipping to the SW as the Eridanos River was supplementing sediments from the NE and later from the East to the North Sea Basin. The sediments above unit 11 (unit 12 and upwards sequences) show an aggradation sequence as the basin was already filled.
- More than 20 wells were studied in terms of their petrophysical characters interpreted from their wireline logs. Seven wells with cores in the North Sea shallow sediments were studied in terms of their sedimentological description, core plugs lab measurements and thin sections. Nine wells were studied in terms of their gas test and shows represented by mudgas interpretation and available production tests. A study of production data from three fields from blocks A12, A18 and B13 was carried out by averaging the horizontal wells' production to show the flow capacity of the gas in the North Sea shallow reservoirs.
    - Cores in the shallow section show alternation between very fine sediments and coarser grains, which is attributed to the switch in climate between cold and warmer conditions. Coarser grains are majorly sands and silts, which make up the reservoir hosting the gas in the shallow North Sea section. Layers of shale above these reservoirs is considered the main seal.
    - Two plots were constructed based on the core measurements of porosity and permeability. One illustrates the variation of porosity with depth and it shows that despite the change in depth, within the reservoir intervals, porosity always ranges form 25 – 45%. The second plot investigates the relation between permeability and porosity, which is found to be directly proportional. Range of different permeability values is observed in intervals with the same porosity. While the relation between porosity and permeability is complex, some variations are explained by clay filling especially in the zones with intense burrows, which is observed from the thin sections.
    - Interpretation of age and depositional environment of the different units was made based on three major groups of fossils, which are Dinoflagellate cysts (Dinocyst), pollen and foraminifers. These fossils are good biomarkers as they are sensitive to changes in environmental parameters such as sea surface temperature, state of the ocean, salinity and vegetation.

- Sedimentation rate of the seismic units was plotted based on the volumes measured in the study by Overeem (2001) and the age controls by Kuhlamnn (2006) and Verreussel & Jansen (1999). Three rates were compared in terms of their differences and similarities and are found to have the same trend of increase in seismic units (5 – 7). The sedimentation rate based on the age controls of Verreussel & Jansen is found to give an anomaly reaching around $10^3 km^3/Ma$, which lacks evidence of any factor that increased the sediment supply dramatically during the time.
- Horizontal shift of the delta was plotted by measuring the progradation distance for the shelf breaks of the seismic units in the three regional 2D lines, that are NE – SW oriented. The results show a maximum shift in units 6 & 7 which align with the highest sedimentation rates of the units.
- Reasoning of the success in some wells for gas in the shallow section (< 1km) of the North Sea Basin was assessed in terms of common factors in the producing wells using both seismic and well data and three main factors were identified:
  - Presence of effective reservoirs and seal have to coexist, as the petroleum system is based on alternation between very fine grains (shales), that are capping the gas, and rocks with coarser grains (sands and silts), that are hosting the gas.
  - A trapping mechanism have to be present, which in the study area is represented by the pre-existing salt domes that insured anticlinal configuration to trap the gas.
  - Source rock and migration paths presence are the main controls of the localization of the gas accumulations around the A and B blocks. A direct relation between gas chimneys and gas fields is found. This relation is explained by the presence of producing fields only above those chimneys as those create migration paths and fracturing to supplement the shallow reservoirs with gas from deeper source rocks.
- A 3D model of the reservoir facies was created by integrating the results of the study. The lithofacies at well location were created based on well cutting samples. Extrapolation/interpolation of those data points was made using Sequential Gaussian Simulation (SGS) and the trend used to guide the lithology distributions and lateral extent was derived from seismic data by creating velocity models of each unit and link lithologies to their corresponding amplitudes from seismic. For mapping the reservoir petrophysical properties:
  - Calculation of porosity and permeability was done by calibrating wireline logs to core measurements and choosing the best fit.
  - Those petrophysical properties where linked to the generated lithologies, in which only reservoir facies were given values (shales/clays were excluded from porosity and permeability extrapolations).

Reference

Abdulkadir, M.O. (2016). *Fundamental of Soil Science, Chapter Two: Soil Physical Properties*. Thelemon Production. pp. 27 – 62.

Anovitz, L.M. & Cole, D.R. (2015). *Characterization and Analysis of Porosity and Pore Structures*. Mineralogical Society of America: Reviews in Mineralogy and Geochemistry. Vol. 80, pp. 61 – 164.

Brown, S. (1990). *Introduction to the Petroleum Geology of the North Sea*. Oxford, Blackwell Scientific Publications. pp. 220-250.

Cameron, D., Van Doorn, D., Laban, C., & Streif, H. (1993). *Geology of the Southern North Sea*. American Shore and Beach Preservation Association ASCE. Louisiana. pp. 14-20.

Catuneanu, O. (2002). *Sequence Stratigraphy of Clastic Systems: Concepts, Merits, and Pitfalls*. Journal of African Earth Sciences, volume 35, pp. 1 – 43.

Catuneanu, O. (2006). *Principles of Sequence Stratigraphy*. ELSEVIER, Amsterdam. pp.235 – 279.

Connolly, D. L., Ghahfarokhi, P. K. & Rosendaal, E. (2015). *Determining the Origin of Shallow Gas in the Dutch North Sea Using Gas Chimney Detection: Implications for Deep Exploration*. AAPG Annual Convention and Exhibition, Denver, CO.

Cunningham A.D. & Droxler A.W. (2000). *Synthetic Seismogram Generation and Seismic Facies to Core Lithology Correlation for Sites 998, 1000, and 1001*. Proceedings of the Ocean Program, Scientific Results, Vol. 165. pp. 205-217.

Delbari, M., Afrasiab, P. & Loiskandl, W. (2009). *Using Sequential Gaussian Simulation to Assess the Filed-scale Spatial Uncertainty of Soil Water Content*. ELSEVIER: CATENA, Vol. 79, Issue, 2, pp. 163 – 169.

Eberli, G.P., Anselmetti, F.S., Kroon, D., Sato, T. & Wright, J.D. (2002). *The Chronostratigraphic Significance of Seismic Reflections along the Bahamas Transect*. ELSEVIER: Marine Geology 185, pp. 1-17.

Fisher, M. & Mudge, D. (1990). *Introduction to the Petroleum Geology of the North Sea*. Oxford, Blackwell Scientific Publication. pp. 191-200.

Fristad, P & Constable, M. V. (2012). *Introduction to Petrophysics*. Exploration and Petroleum Technical & IOR Networks: Statoil.

Gibbard, P. & Lewin, J. (2014). *Filling the North Sea Basin: Cenozoic Sediment Sources and River Styles*. Geologica Belgica 19/3-4: pp. 201-2017.

Gibbard, P. (1988). *The History of the Great Northwest European Rivers During the Past Three Million Years*. London B. pp. 559-600.

Gibson, C. H. (1980). *Fossil Temperature, Salinity, and Vorticity Turbulence in the Ocean*. Elsevier Oceanography Series. Volume 28, pp. 221-257

Glennie, K. (1990). *Introduction to Petroleum Geology of the North Sea*. Oxford, Blackwell Scientific Publications. pp. 36-70.

Glover, P.W.J. (2000). *Formation Evaluation*. Department of Geology and Petroleum Geology: University of Aberdeen, UK. pp. 55-64.

Guion, P. & Fielding, C. (1988). *Sedimentation in a Synorogenic Basin Complex: The Upper Carboniferous of Northwest Europe*. London, Blackie & Son. pp. 153-177.

Herngreen, G. & Wong. E (1987). *Revision of the Late Jurassic Stratigraphy of the Dutch Central Sea Graben*. Geol. Mijnb. pp. 73-100.

Hillis, R., Holford, S., Green, P., Dore, A. Gatliff, R., Stoker, M., Thomson, K., Turner, J., Underhill, J. & Williams, G. (2008). *Cenozoic Exhumation of the Southern British Isles*. Geology (2008) 36 (5): pp. 371-374.

Japsen, P., Green, P., Nielsen, L. Rasmussen, E & Bidstrup, T. (2007). *Mesozoic-Cenozoic Exhumation Events in the Easter North Sea Basin: A Multi-disciplinary Study Based on Palaeotheraml, Palaeoburial, Stratgraphic and Seismic Data.* EAGE. Volume 19, Issue 4. pp. 451-490.

Jilani, S. Z., Menouar, M., Al-Majed, A. A. And Khan, M. A. (2002). *Effect of Overbalance Pressure on Formation Damage*. Elsevier, Journal of Petroleum Science and Engineering volume 36 pp. 97–109.

Knox, R., Bosch, J., Rasmussen, E., Heilmann-Clausen, C., Hiss, M., De Lugt, I., Kasinksi, J., King, C. Kothe, A., Slodkowska, B., Standke, G. & Vandenberghe, N. (2010). *Petroleum Geology Atlas of the Southern Permian Basin Area: Cenozoic*. EAGE, Houten. Chapter 12, 211-223.

Kooi, H., Cloetingh, S. & Remmelts, G. (1989). *Intraplate Stresses and the Stratigraphic Evolution of the North Sea Central Graben*. Geol. Mijnb. pp. 49-69.

Koson, S., Chenrai. P. & Choowong, M. (2014). *Seismic Attributes and Seismic Geomorphology*. Bulletin of Earth Sciences of Thailand. Volume 6, number 1, pp. 1-9.

Kuhlmann, G. & Wong, T.E. (2008). *Pliocene Paleoenvironment Evolution as Interpreted from 3D-Seismic Data in the Southern North Sea, Dutch Offshore Sector*. ELSEVIER, Marine and Petroleum Geology 25 , pp.173-189.

Kuhlmann, G., Langereis, C., Munsterman, D., Jan van Leeuwen, R., Verreussel, R., Meulenkamp, J. & Wong, T. (2006). *Chronostratigraphy of Late Neogene Sediments in the Southern North Sea Basin and Paleoenvironmental Interpretations*. ELSEVIER, Palaeoecology 239, pp. 426-455.

Leeder, M. (1987). *Tectonic and Paleogeographic Model for Lower Carboniferous Europe*. Chichester, John Whiley & Sons. pp-1-20.

Lidmar-Bergstorm, K., Ollier, C. & Sulebac, J. (2000). *Global and Planetary Change: Landforms and Uplift History of Southern Norway*. ELSEVIER, volume 24, issues 3-4. pp. 211-231.

Livingstone, S. J. & Clark, C. D. (2016). *Morphological properties of tunnel valleys of the southern sector of the Laurentide Ice Sheet and implications for their formation*. Department of Geography, University of Sheffield, Sheffield, S10 2TN, UK. Earth Surf. Dynam., 4, pp. 567–589.

Mahbaz, S., Sardar, H., Namjouyan, M. & Mirzaahmadian, Y. (2011). *Optimization of Reservoir Cut-off Parameters: A Case Study in SW Iran*. EAGE: Petroleum Geoscience, Vol. 17 2011, pp. 355–363.

Marzec, P., Sechman, H., Kasperska, M., Cichostepski. K., Guzy, P. & Pietsch, K. (2016). *Interpretation of a Gas Chimney in the Polish Carpathian Foredeep based on Integrated Seismic and Geochemical Data*. Basin research, volume 30, issue S1.

Miller, K., Mountain, G., Browning, J., Kominz, M. Sugarman, P., Christi-Blick, N. Katz, M. & Wright J. (1988). *Cenozoic Global Seal Level, Sequence and the New Jersey Transect: Results from Coastal Plain and Slope Drilling*. Reviews of Geophysics. Volume 36, issue 4. pp. 359-601.

Mode, A. W., Anyiam, O. A., Egbujie, B. C. (2014). *The Application of Chromatographic Gas Ratio Analysis in ReservoirFluid Evaluation of "Beta" Field in the Congo Basin*. Journal Geological Society of India. Vol. 84, pp. 303-310.

Muller, S., Reinhardt, L., Franke, D., Gaedicke, C. & Winsmann, J. (2018). *Shallow gas accumulations in the German North Sea*. ELSEVIER: Marine and Petroleum Geology 9, pp. 139-151.

Nietzsche, F. (2005). *Common Techniques for Quantitative Seismic Interpretation*. Published by Cambridge University Press. pp. 168-257.

Overeem, G., Weltje, C., Bishop-Kayt, C. & Kroonenberg, S. (2001). *The Late Cenozoic Eridanos Delta System in the Southern North Sea Basin: A Climate Signal in Sediment Supply*. Applied Earth Scieneces: Delft University of Technology, The Netherlands. Woodside Energy Ltd, Perth, Australia. pp. 292-297.

Rafaelsen. B (2006). *Seismic resolution (and frequency filtering).* University of Tromsø.

Sandersen, P. B. E & Jorgensen, F. (2012). *Substratum Control on Tunnel Valley Formation in Denmark*. Geological Society, London. Doi:10.1144/SP368.12.

Schroot, B.M. & Schuttenhelm R.T.E. (2003). *Expressions of Shallow Gas in the Netherlands North Sea*. Netherlands Journal of Geoscience: Geologie en Mijnbouw 82 (1), pp. 91-105.

Schroot, B.M. Klaver, G.T. & Schuttenhelm R.T.E. (2005). *Surface and Subsurface expressions of Gas Seepage to the Seabed: Examples from the Southern North Sea*. Marine and Petroleum Geology 22, pp 499-515.

Seranne, M., Nze Abeigne, C.R. & Lopez. M. (2000). *Reply to 'Oligocene to Holocene sediment drifts and bottomcurrents on the slope of Gabon continental margin (West Africa). Consequences for sedimentation and southeast Atlantic upwelling'*. Sedimentary Geology 136, pp. 163-168.

Serra, O. (1984). *Fundamentals of Well-log Interpretation: The Acquisition of Logging Data*. ELSVIER, Developments in Petroleum Science, 15A.

Sorensen, J., Gregersen, U., Breiner, M & Michelsen, O. (1997). *High Frequency Sequence Stratigraphy of Upper Cenozoic Deposits in the Central and Southeastern North Sea Areas*. ELSEVIER Science Ltd. Marine and Petroleum Geology, Vol. 14, No. 2. pp. 99-123.

Stuart, J.Y. & Huuse, M. (2012). *3D Seismic Geomorphology of a Large Plio-Pleistocene Delta 'Bright Spots' and Contourites in the Southern North Sea*. ELSEVIER, Marine and Petroleum Geology 38, pp. 143-157.

Subrahmanyam, D. & Rao, P.H. (2008). *Seismic Attributes- A Review*. Seventh International Conference & Exposition on Petroleum Geophysics.

Ten Veen, J.H, Verweij, H., Donders, T., Geel, K., De Bruin, G., Munsterman, D., Verreussel, R., Daza Cajigal, V., Harding, R. & Cremer H. (2013). *Anatomy of the Cenozoic Eridanos Delta Hydrocarbon System*. TNO, Earth, Environmental and Life Sciences, Utrecht, The Netherlands. TNO 2013 R10060.

Van Den Belt, F.J.G. & Van Dijk, C.P.J. (2000). *Sedimentology and Petrography of Upper North Sea Group: Well A15-3*. Prepared by PANterra for Wintershall Noordzee B.V. The Netherlands.

Verreussel, R. & Jansen, H. (1999). *Biostratigraphy of Wintershall's A15-3 Well*. J&G and LPP. Heemstede, Utrecht.

Yan, J. (2001). *Reservoir Parameters Estimation from Well Log and Core Data: A Case Study from the North Sea*. British Geological Survey, Edinburgh, Scotland, UK.

Yuwono, R. W., Fitriana, B. S., Kirana, P. S., Djaelani, S. & Sjafwan, B. A. (2012). *Biogenic Gas Exploration and Development in Bentu PSC, Central Sumatra Basin, Indonesia*. Search and Discovery Article #10454: Adopted from AAPG International Conference and Exhibition, Singapore.

Ziegler. P (1990). *Geological Atlas of Western and Central Europe*. Amsterdam, 778 Shell International Maatschappij BV.

Appendix A (Seismic structure maps)

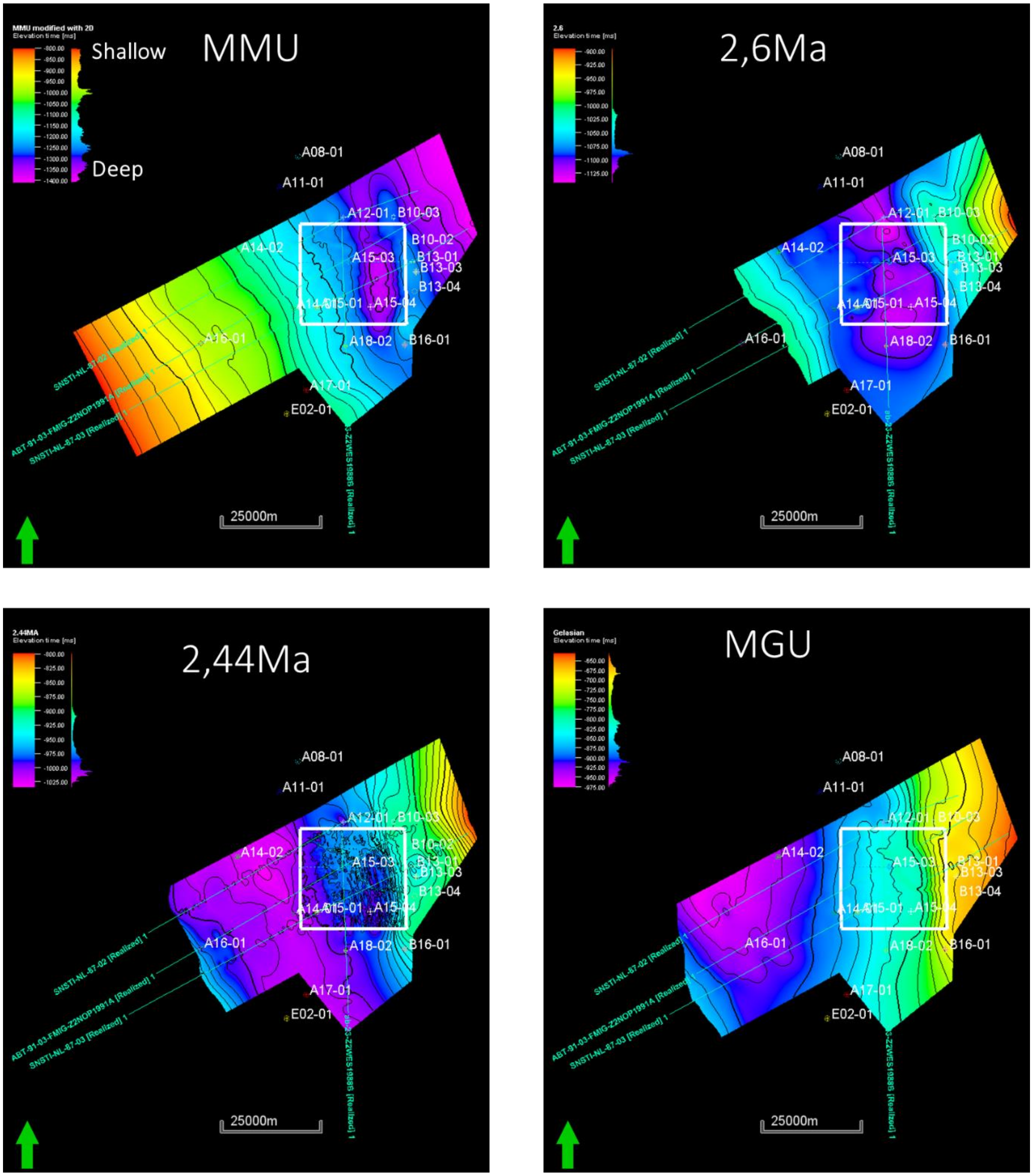

Appendix A 1: Seismic structure maps in time for MMU - MGU.

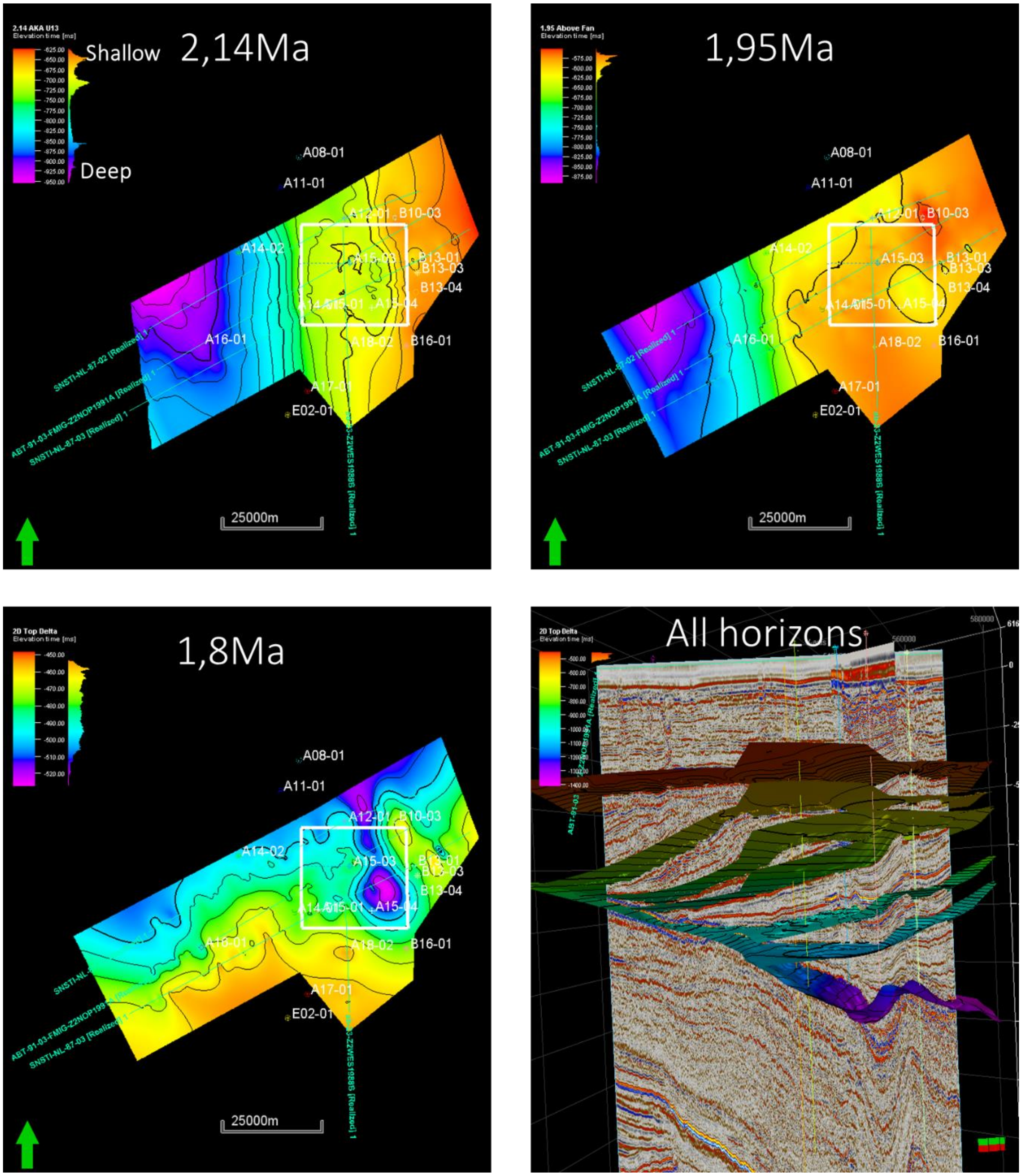

Appendix A 2: Seismic structure maps in time for 2.14 – 1.8 Ma.

Appendix B (Seismic Isochrone maps)

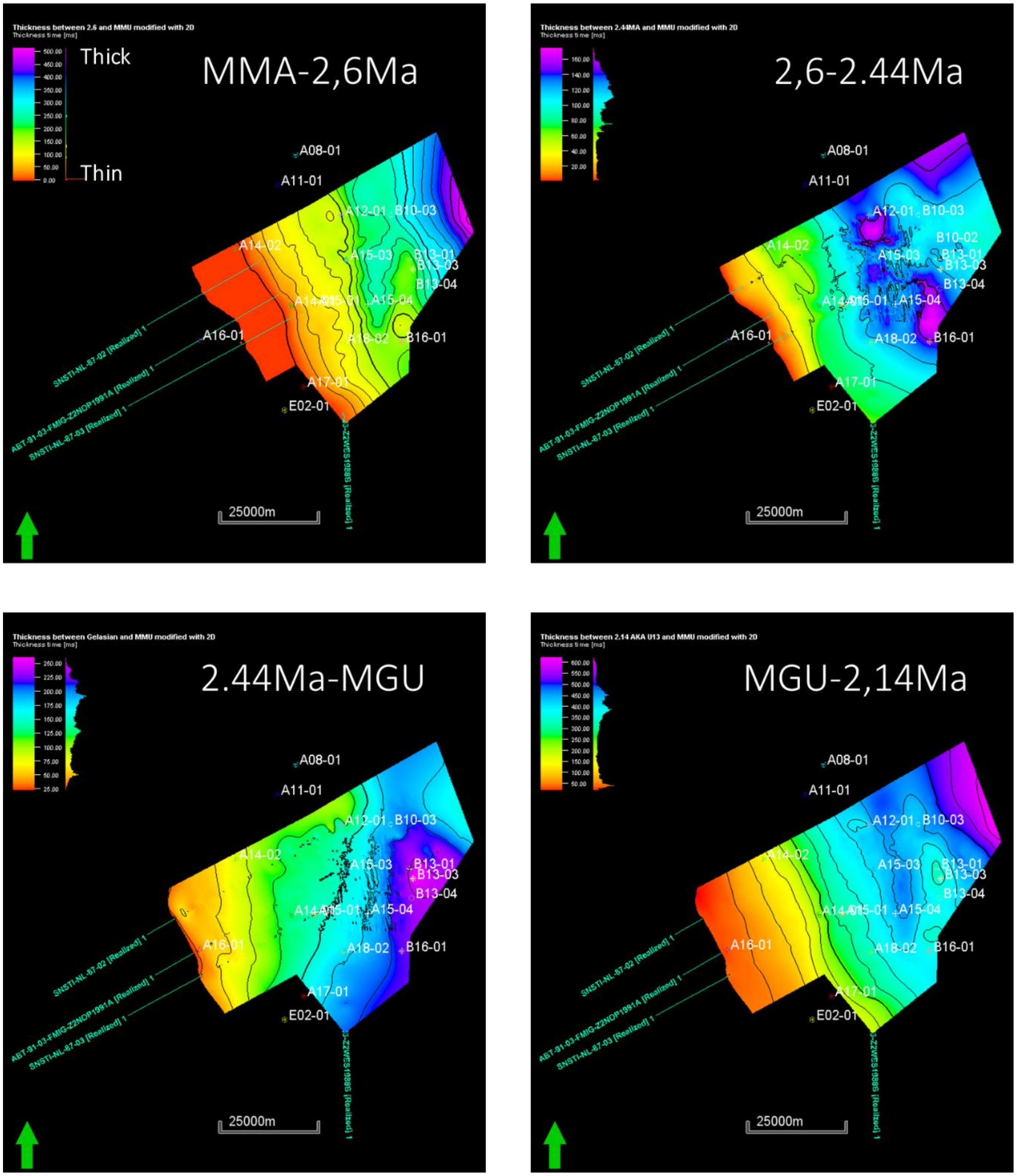

Appendix B 1: Seismic Thickness maps in time MMA – 2.14 ma.

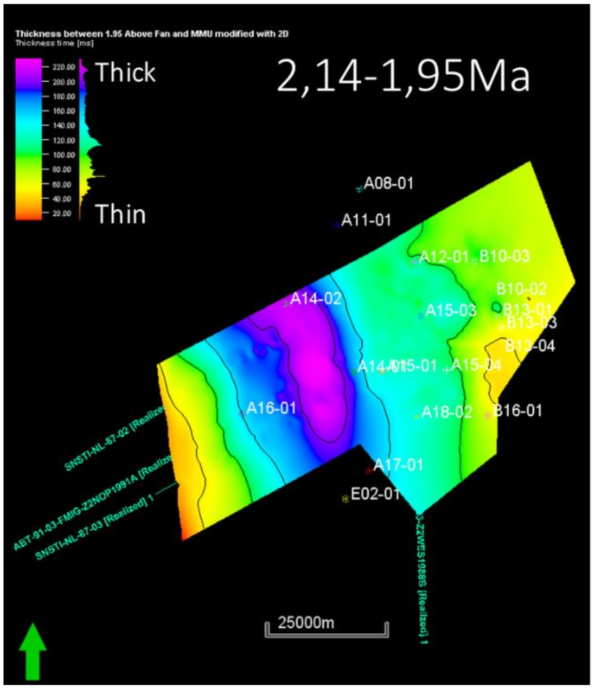

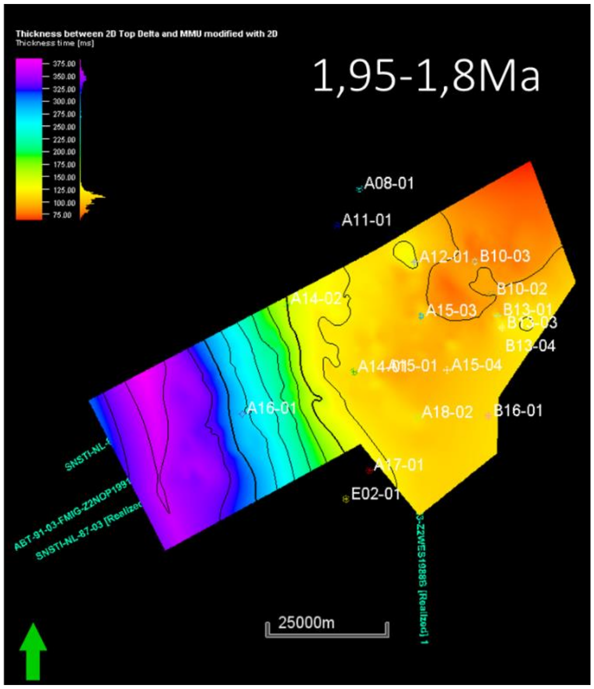

Appendix B 2: Seismic thickness maps in time 2.14 - 1.8 Ma.

Appendix C (3D modeling)

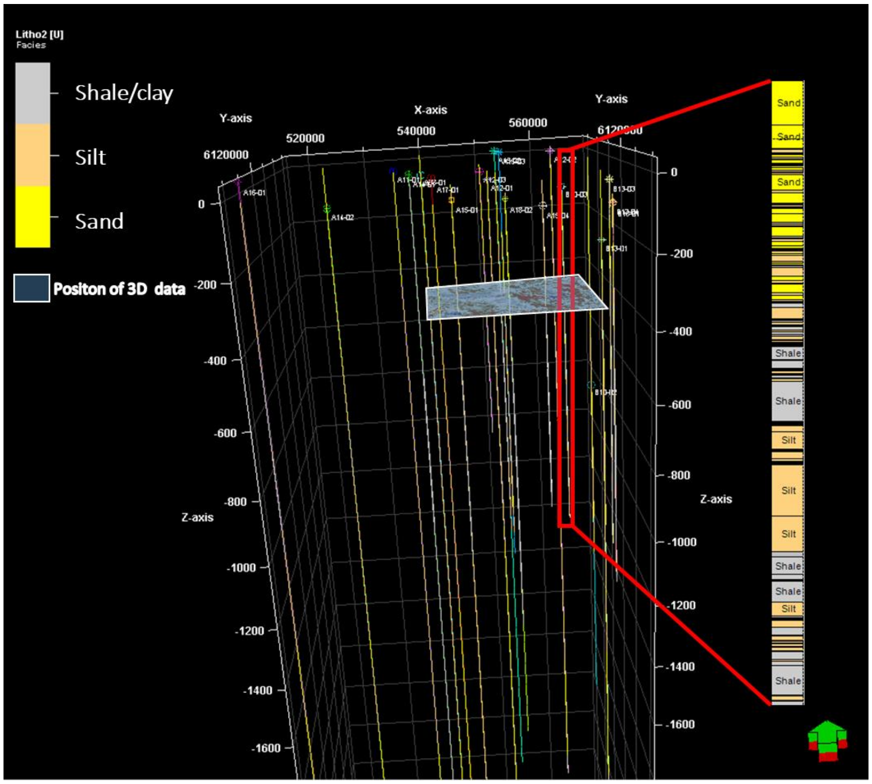

Appendix C 1: Wells' lithology creation using cutting samples.

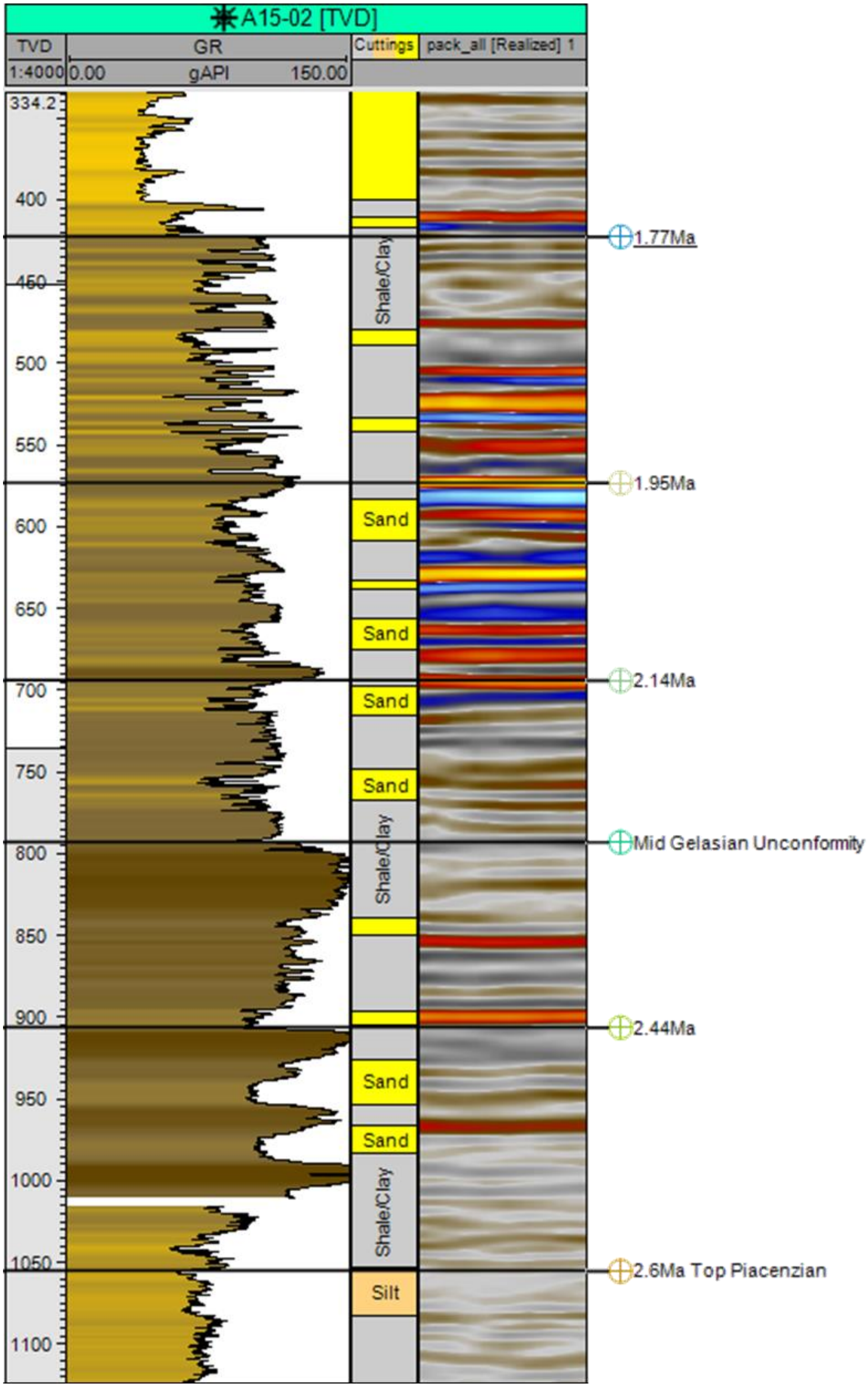

Appendix C 2: lithofacies and their seismic amplitudes reflection equivalent.

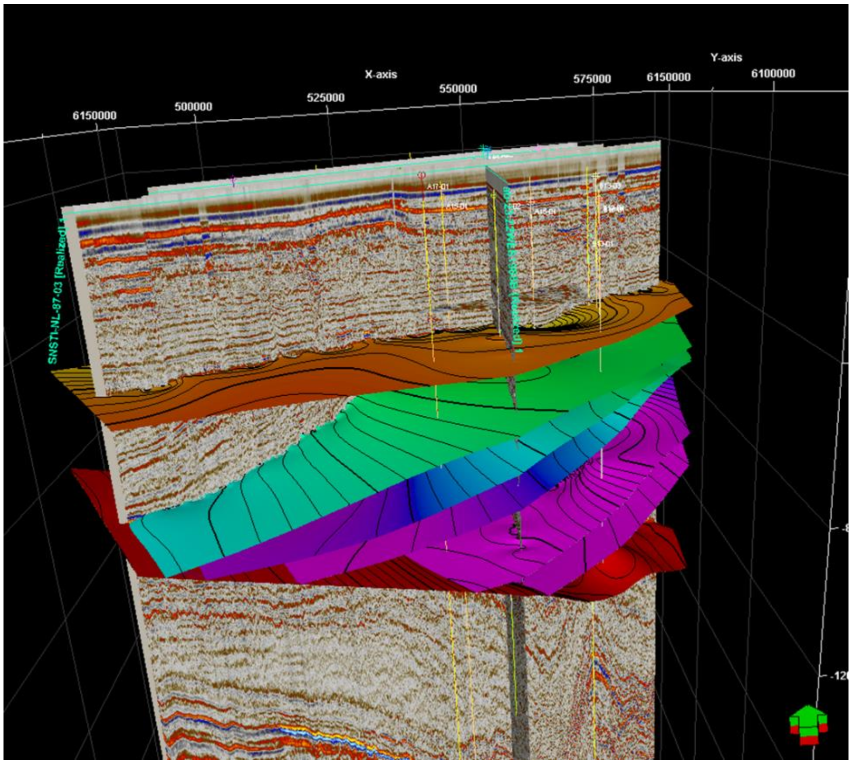

Appendix C 3: Seismic structure maps incorporation in the 3D model for trend guidance.

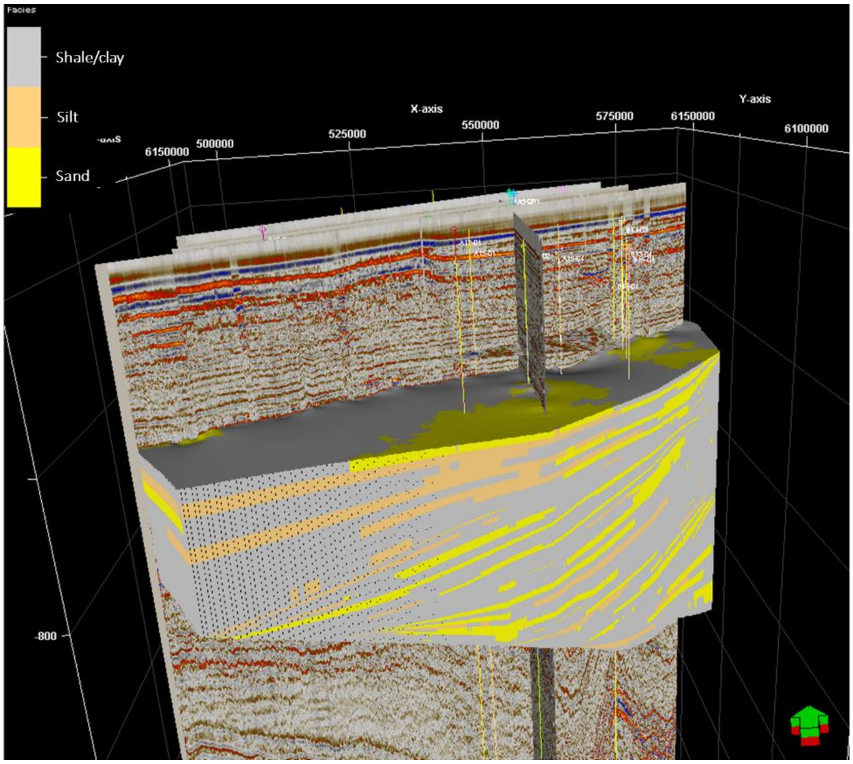

Appendix C 4: Lithology extrapolation using seismic trend.

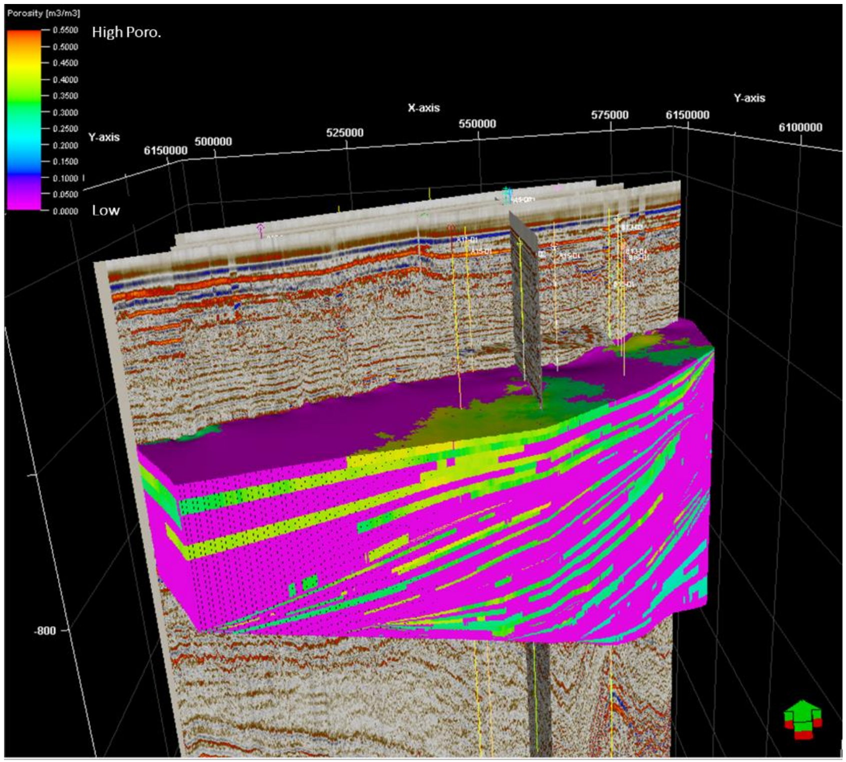

Appendix C 5: Petrophysical properties porosity modeling for the reservoir zones.

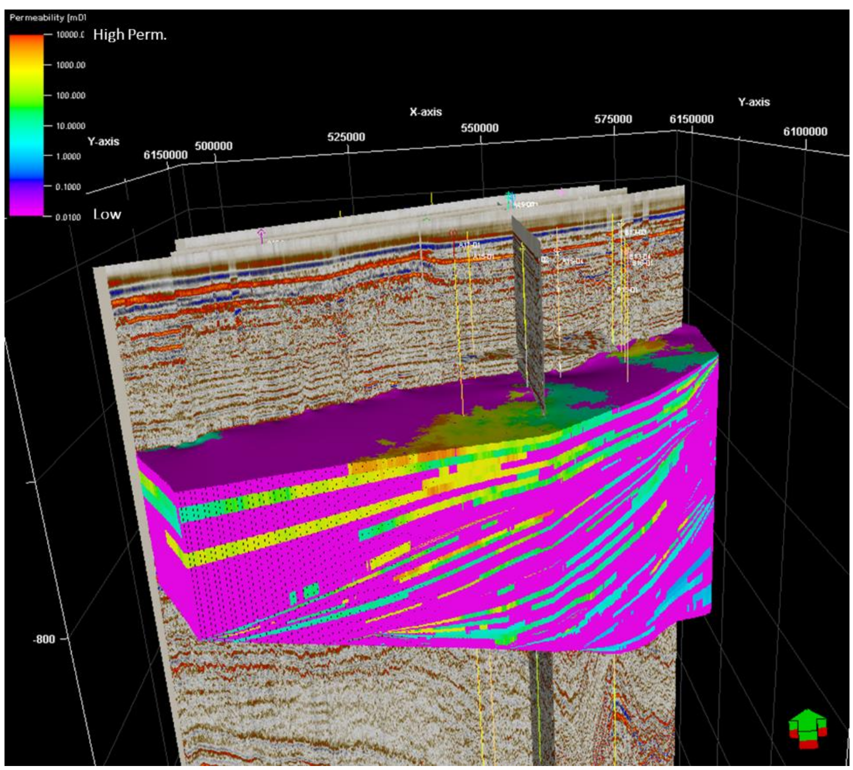

Appendix C 6: Petrophysical properties permeability modeling for the reservoir zones.